

# UCSF

## UC San Francisco Previously Published Works

### Title

Methodological consensus on clinical proton MRS of the brain: Review and recommendations.

### Permalink

<https://escholarship.org/uc/item/15m1p6w0>

### Journal

Magnetic resonance in medicine, 82(2)

### ISSN

0740-3194

### Authors

Wilson, Martin  
Andronesi, Ovidiu  
Barker, Peter B  
et al.

### Publication Date

2019-08-01

### DOI

10.1002/mrm.27742

Peer reviewed

## REVIEW

# Methodological consensus on clinical proton MRS of the brain: Review and recommendations

Martin Wilson<sup>1</sup>  | Ovidiu Andronesi<sup>2</sup> | Peter B. Barker<sup>3</sup> | Robert Bartha<sup>4</sup> | Alberto Bizzi<sup>5</sup> | Patrick J. Bolan<sup>6</sup> | Kevin M. Brindle<sup>7</sup> | In-Young Choi<sup>8</sup> | Cristina Cudalbu<sup>9</sup> | Ulrike Dydak<sup>10</sup> | Uzay E. Emir<sup>10</sup> | Ramon G. Gonzalez<sup>11</sup> | Stephan Gruber<sup>12</sup> | Rolf Gruetter<sup>13</sup> | Rakesh K. Gupta<sup>14</sup> | Arend Heerschap<sup>15</sup> | Anke Henning<sup>16</sup> | Hoby P. Hetherington<sup>17</sup> | Petra S. Huppi<sup>18</sup> | Ralph E. Hurd<sup>19</sup> | Kejal Kantarci<sup>20</sup> | Risto A Kauppinen<sup>21</sup> | Dennis W. J. Klomp<sup>22</sup> | Roland Kreis<sup>23</sup>  | Marijn J. Kruiskamp<sup>24</sup> | Martin O. Leach<sup>25</sup> | Alexander P. Lin<sup>26</sup> | Peter R. Luijten<sup>22</sup> | Małgorzata Marjańska<sup>6</sup> | Andrew A. Maudsley<sup>27</sup>  | Dieter J. Meyerhoff<sup>28</sup> | Carolyn E. Mountford<sup>29</sup> | Paul G. Mullins<sup>30</sup> | James B. Murdoch<sup>31</sup> | Sarah J. Nelson<sup>32</sup> | Ralph Noeske<sup>33</sup> | Gülin Öz<sup>6</sup> | Julie W. Pan<sup>34</sup> | Andrew C. Peet<sup>35</sup> | Harish Poptani<sup>36</sup> | Stefan Posse<sup>37</sup> | Eva-Maria Ratai<sup>2</sup> | Nouha Salibi<sup>38</sup> | Tom W. J. Scheenen<sup>15</sup> | Ian C. P. Smith<sup>39</sup> | Brian J. Soher<sup>40</sup> | Ivan Tkáč<sup>6</sup> | Daniel B. Vigneron<sup>32</sup> | Franklyn A. Howe<sup>41</sup> 

<sup>1</sup>Centre for Human Brain Health and School of Psychology, University of Birmingham, Birmingham, England

<sup>2</sup>Martinos Center for Biomedical Imaging, Department of Radiology, Massachusetts General Hospital, Harvard Medical School, Boston, Massachusetts

<sup>3</sup>Department of Radiology, Johns Hopkins University School of Medicine, Baltimore, Maryland

<sup>4</sup>Robarts Research Institute, University of Western Ontario, London, Canada

<sup>5</sup>U.O. Neuroradiologia, Fondazione IRCCS Istituto Neurologico Carlo Besta, Milano, Italy

<sup>6</sup>Department of Radiology, Center for Magnetic Resonance Research, University of Minnesota, Minneapolis, Minnesota

<sup>7</sup>Department of Biochemistry, University of Cambridge, Cambridge, England

<sup>8</sup>Department of Neurology, Hogle Brain Imaging Center, University of Kansas Medical Center, Kansas City, Kansas

<sup>9</sup>Center for Biomedical Imaging, Ecole Polytechnique Federale de Lausanne, Lausanne, Switzerland

<sup>10</sup>School of Health Sciences, Purdue University, West Lafayette, Indiana

<sup>11</sup>Department of Radiology, Massachusetts General Hospital, Harvard Medical School, Boston, Massachusetts

<sup>12</sup>High Field MR Center, Department of Biomedical imaging and Image-Guided Therapy, Medical University of Vienna, Vienna, Austria

<sup>13</sup>Laboratory for Functional and Metabolic Imaging, Center for Biomedical Imaging, Ecole Polytechnique Federale de Lausanne, Lausanne, Switzerland

<sup>14</sup>Fortis Memorial Research Institute, Gurugram, Haryana, India

<sup>15</sup>Department of Radiology and Nuclear Medicine, Radboud University Medical Center, Nijmegen, the Netherlands

<sup>16</sup>Max Planck Institute for Biological Cybernetics, Tuebingen, Germany

<sup>17</sup>Department of Radiology, University of Pittsburgh, Pittsburgh, Pennsylvania

<sup>18</sup>Department of Pediatrics, University of Geneva, Geneva, Switzerland

<sup>19</sup>Stanford Radiological Sciences Lab, Stanford, California

<sup>20</sup>Department of Radiology, Mayo Clinic, Rochester, Minnesota

<sup>21</sup>School of Psychological Science, University of Bristol, Bristol, England

<sup>22</sup>University Medical Centre Utrecht, Utrecht, the Netherlands

<sup>23</sup>Departments of Radiology and Biomedical Research, University of Bern, Bern, Switzerland

<sup>24</sup>Philips Healthcare, Best, the Netherlands

<sup>25</sup>CRUK Cancer Imaging Centre, Institute of Cancer Research and Royal Marsden Hospital, London, England

<sup>26</sup>Center for Clinical Spectroscopy, Brigham and Women's Hospital, Harvard University Medical School, Boston, Massachusetts

<sup>27</sup>Department of Radiology, University of Miami, Miami, Florida

<sup>28</sup>DVA Medical Center and Department of Radiology and Biomedical Imaging, University of California San Francisco, San Francisco, California

<sup>29</sup>Translational Research Institute, Woolloongabba, Australia

<sup>30</sup>Bangor Imaging Unit, School of Psychology, Bangor University, Bangor, Wales

<sup>31</sup>Canon Medical Research USA, Mayfield Village, Ohio

<sup>32</sup>Department of Radiology and Biomedical Imaging, University of California San Francisco, San Francisco, California

<sup>33</sup>GE Healthcare, Berlin, Germany

<sup>34</sup>Department of Neurology, University of Pittsburgh, Pittsburgh, Pennsylvania

<sup>35</sup>Institute of Cancer and Genomic Sciences, University of Birmingham, Birmingham, England

<sup>36</sup>Centre for Preclinical Imaging, Institute of Translational Medicine, University of Liverpool, Liverpool, England

<sup>37</sup>Department of Neurology, University of New Mexico, Albuquerque, New Mexico

<sup>38</sup>MR R&D, Siemens Healthineers, Malvern, Pennsylvania

<sup>39</sup>Innovative Bidiagnostics, Winnipeg, Canada

<sup>40</sup>Department of Radiology, Duke University Medical Center, Durham, North Carolina

<sup>41</sup>Molecular and Clinical Sciences, St George's University of London, London, England

#### Correspondence

Martin Wilson, Centre for Human Brain Health, University of Birmingham, Edgbaston, Birmingham B15 2TT, England.  
Email: wilsonmp@bham.ac.uk  
Twitter: @martinw3141

Proton MRS (<sup>1</sup>H MRS) provides noninvasive, quantitative metabolite profiles of tissue and has been shown to aid the clinical management of several brain diseases. Although most modern clinical MR scanners support MRS capabilities, routine use is largely restricted to specialized centers with good access to MR research support. Widespread adoption has been slow for several reasons, and technical challenges toward obtaining reliable good-quality results have been identified as a contributing factor. Considerable progress has been made by the research community to address many of these challenges, and in this paper a consensus is presented on deficiencies in widely available MRS methodology and validated improvements that are currently in routine use at several clinical research institutions. In particular, the localization error for the PRESS localization sequence was found to be unacceptably high at 3 T, and use of the semi-adiabatic localization by adiabatic selective refocusing sequence is a recommended solution. Incorporation of simulated metabolite basis sets into analysis routines is recommended for reliably capturing the full spectral detail available from short TE acquisitions. In addition, the importance of achieving a highly homogenous static magnetic field ( $B_0$ ) in the acquisition region is emphasized, and the limitations of current methods and hardware are discussed. Most recommendations require only software improvements, greatly enhancing the capabilities of clinical MRS on existing hardware. Implementation of these recommendations should strengthen current clinical applications and advance progress toward developing and validating new MRS biomarkers for clinical use.

#### KEYWORDS

brain, consensus, metabolites, MRS, semi-LASER, shimming

## 1 | INTRODUCTION

Proton MRS ( $^1\text{H}$  MRS) has provided a noninvasive measure of brain metabolites since the late 1980s. Abnormal metabolism is often closely linked to disease processes; therefore, MRS may improve clinical diagnosis, treatment effect monitoring, and understanding of disease mechanisms.<sup>1</sup> However, widespread clinical adoption has been slow, with MRS being used primarily in specialized imaging centers.

Increased availability of 3T MR scanners in hospitals presents an important opportunity for MRS, as metabolite levels are more reliably measured than at 1.5 T due to reduced spectral overlap and an improved SNR (Figure 1).<sup>2</sup> However, additional challenges are associated with 3T MRS compared with 1.5 T. Reduced homogeneity of the static magnetic field ( $B_0$ ) at 3 T results in broadened spectral linewidths and degraded spectral quality; therefore, improvements in hardware and methodology for optimizing the  $B_0$  homogeneity over the region for MRS are necessary. Metabolite localization errors, known as chemical shift displacement (CSD), also increase at 3 T, requiring optimized RF pulse shapes and higher  $B_1$  RF power to compensate. Recent progress in the research community has addressed these challenges, but a major disparity remains between what is available for research and for routine clinical applications. In addition, the wide range of MRS sequences, parameters, and analysis choices can make the technique particularly difficult for nonexpert users.

This paper was written and agreed upon by 49 MRS experts who belong to the International Society for Magnetic Resonance in Medicine (ISMRM) MRS study group with the following aims:

1. Recommend appropriate methodology to improve the quality of future MRS studies and increase MRS standardization, to facilitate clinical trials and meta-analyses of MRS efficacy;
2. Provide recommendations to vendors regarding the best MRS implementations and practices; and
3. Focus the research community on resolving key technical barriers that have delayed wider clinical adoption of MRS.

Following initial discussions, an online survey was designed and completed by the group, and the results (Supporting Information Section A) were used to guide further discussions leading to our final consensus and recommendations. We restricted our scope to  $^1\text{H}$  MRS detection of endogenous brain metabolites, using currently available methodologies that we believe are ready for incorporation into clinical scanner platforms. We first present a basic introduction to  $^1\text{H}$  MRS methodology that is designed to give newcomers to  $^1\text{H}$  MRS sufficient background to understand the subsequent consensus sections.

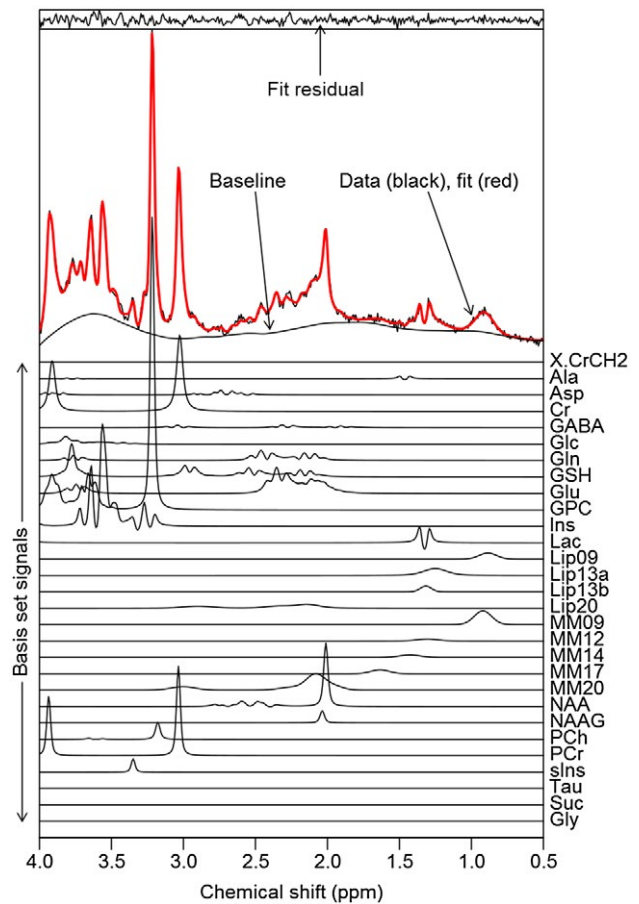


**FIGURE 1** An adult low-grade glioma brain tumor spectrum acquired at 3 T with PRESS single-voxel spectroscopy (SVS) localization, 18-mm-sided cubic voxel, 128 averages, TE = 32 ms, and TR = 2 seconds. Parametric fitting was performed with the TARQUIN algorithm<sup>35</sup> using a simulated basis set of metabolite, lipid, and macromolecule signals. Although a greater level of spectral detail is available when compared with 1.5 T, particularly for strongly  $J$ -coupled metabolites such as glutamate and *myo*-inositol, data quality is highly dependent on achieving good shimming. For this example, a metabolite FWHM of 0.03 ppm and SNR of 83 were achieved, in which the FWHM was measured from the highest metabolite signal (total choline [tCho] = glycerophosphocholine + phosphorylcholine) following baseline subtraction. The SNR was calculated as the ratio between the highest baseline subtracted, metabolite signal intensity, and 2 times the SD of the noise level estimated from a spectral region free from metabolite signals

## 2 | STANDARD MRS METHODOLOGY

### 2.1 | Single-voxel spectroscopy

Proton single-voxel spectroscopy (SVS) is relatively simple to plan and yields clinically informative results, with robust acquisition procedures available on all commercial systems. Single-voxel spectroscopy is currently the most commonly used method to acquire spectra from a single volume of

interest (VOI or voxel). Generally, a 5-minute acquisition time provides good-quality spectra at 3 T from tissue volumes down to 4 cm<sup>3</sup>, assuming that good B<sub>0</sub> homogeneity can be achieved. We briefly outline the main technical considerations for widely available SVS methodology.

### 2.1.1 | Acquisition methods

Stimulated echo acquisition mode (STEAM)<sup>3,4</sup> and point-resolved spectroscopy (PRESS)<sup>5</sup> are used widely to provide single-shot 3D localization from the intersection of 3 slices. In STEAM, 3 slice-selective RF pulses, each with 90° flip angles, produce a stimulated echo with typically a shortest TE of approximately 20 ms. In PRESS, a 90° excitation pulse combined with 2 refocusing pulses produce a spin echo with a shortest TE of approximately 30 ms. The PRESS refocusing pulses are nominally 180°; however, some implementations use lower flip angles. Shorter TEs are possible for both STEAM and PRESS, but we restrict this section to commercial implementations. The PRESS technique is more commonly used, as its spin echo provides twice the signal compared with the STEAM stimulated echo.

Because multiple averages are typically measured for SVS, the phase of the RF pulses and receiver may be cycled between averages to suppress artifacts from outer-volume signals, imperfect flip angles, and imbalances in scanner electronics—a method known as phase cycling.<sup>6,7</sup> Phase cycling schemes are typically applied in blocks of 2, 4, 8, or 16 averages, which are repeated to attain the desired scan duration. A further method to reduce artifacts originating from outside the prescribed voxel is to ensure that the last slice-selection plane is perpendicular to regions of B<sub>0</sub> inhomogeneity. For example, having the final slice-selection plane in the axial direction has been shown to reduce SVS artifacts in frontal brain regions by eliminating spurious signals caused by B<sub>0</sub> inhomogeneity in the mouth and sinuses.<sup>7,8</sup>

All localization methods based on RF/gradient slice selection, such as PRESS and STEAM, exhibit a localization inaccuracy known as the chemical shift displacement (CSD) error. The CSD error causes a spatial displacement of metabolite resonance localization, in which resonances further from the center frequency of the RF pulse are displaced to a greater extent (Figure 2). Metabolites with frequency-separated *J*-coupled multiplets, such as lactate, may have reduced signal due to regions around the voxel edge periphery not experiencing all 3 localization pulses equally.<sup>9</sup> For a given maximum RF amplitude (B<sub>1max</sub>), the CSD error worsens with increasing field strength and reduced RF pulse bandwidth. Therefore, CSD is worse for PRESS than STEAM, as conventional 90° pulses have greater bandwidth than conventional 180° pulses for a fixed pulse duration and B<sub>1max</sub>. The CSD severity and reduction

will be described in the “Consensus opinion and recommendations” section.

In recent years, the development of the phased-array head coil<sup>10,11</sup> has resulted in improved SNR for MRI and MRS, and modern vendor-supplied MRS protocols at 1.5 T and 3 T are performed using the body (volume) coil for B<sub>1</sub> transmission and a phased-array head coil for B<sub>1</sub> reception. Compared with traditional transmit–receive (T/R) birdcage head coils, the combination of phased-arrayed receive and volume transmit offers improved SNR in cortical brain regions, due to the close proximity of receive coils to cortical areas, and homogeneous B<sub>1</sub> available from the volume transmit coil. In central brain regions, SNR gains are feasible using tighter-fitting receive coils. For well-designed coils and optimized data reconstruction,<sup>12–14</sup> a higher number of array elements should confer improved SNR in cortical regions, with a recent report demonstrating a 40% improvement when using 32 elements compared with 8.<sup>15</sup> One potential disadvantage with using body coils for transmission is reduced B<sub>1max</sub> when compared with T/R designs; however, adequate B<sub>1max</sub> has been demonstrated at 3 T for low CSD sequences (see “Single-voxel spectroscopy acquisition consensus” section). Overall, the use of phased-array head coils with a high number of receive elements is recommended for neuro SVS and MRS imaging (MRSI) at 1.5 T and 3 T.

### 2.1.2 | Repetition time and TE considerations

Proper determination of absolute metabolite concentrations or ratios (e.g., total N-acetylaspartate [tNAA]/total creatine [tCr]) ideally requires long TRs and short TEs to minimize signal loss from T<sub>1</sub> saturation and T<sub>2</sub> relaxation effects, respectively. Short TEs (20–30 ms) also offer improved detection of metabolites with complex *J*-coupled spectral patterns (e.g., glutamine, glutamate, and *myo*-inositol) due to reduced dephasing from *J*-coupling evolution. High-quality short-TE MRS allows the quantification of an extended neurochemical profile, including neurotransmitters and antioxidants.<sup>16</sup> However, a challenge associated with shorter TEs is the enhancement of broad short-T<sub>2</sub> signals from high-molecular-weight macromolecules (MMs) and lipids.<sup>17</sup> Appropriate analysis methods are capable of separating metabolite and lipid/MM signals, but poor B<sub>0</sub> homogeneity degrades this separation; longer TE acquisitions may be used to suppress broad MM and lipid signals, and simultaneously refocus weakly *J*-coupled spins. For instance, a TE of 144 ms or 288 ms is used commonly to aid the discrimination of lactate from lipids and singlets from overlapping multiplets. Although long TRs (> 2 seconds) reduce unwanted signal loss per transient/average from T<sub>1</sub> relaxation effects, the metabolite SNR per unit time is also reduced; therefore, a compromise is often required for clinical MRS.



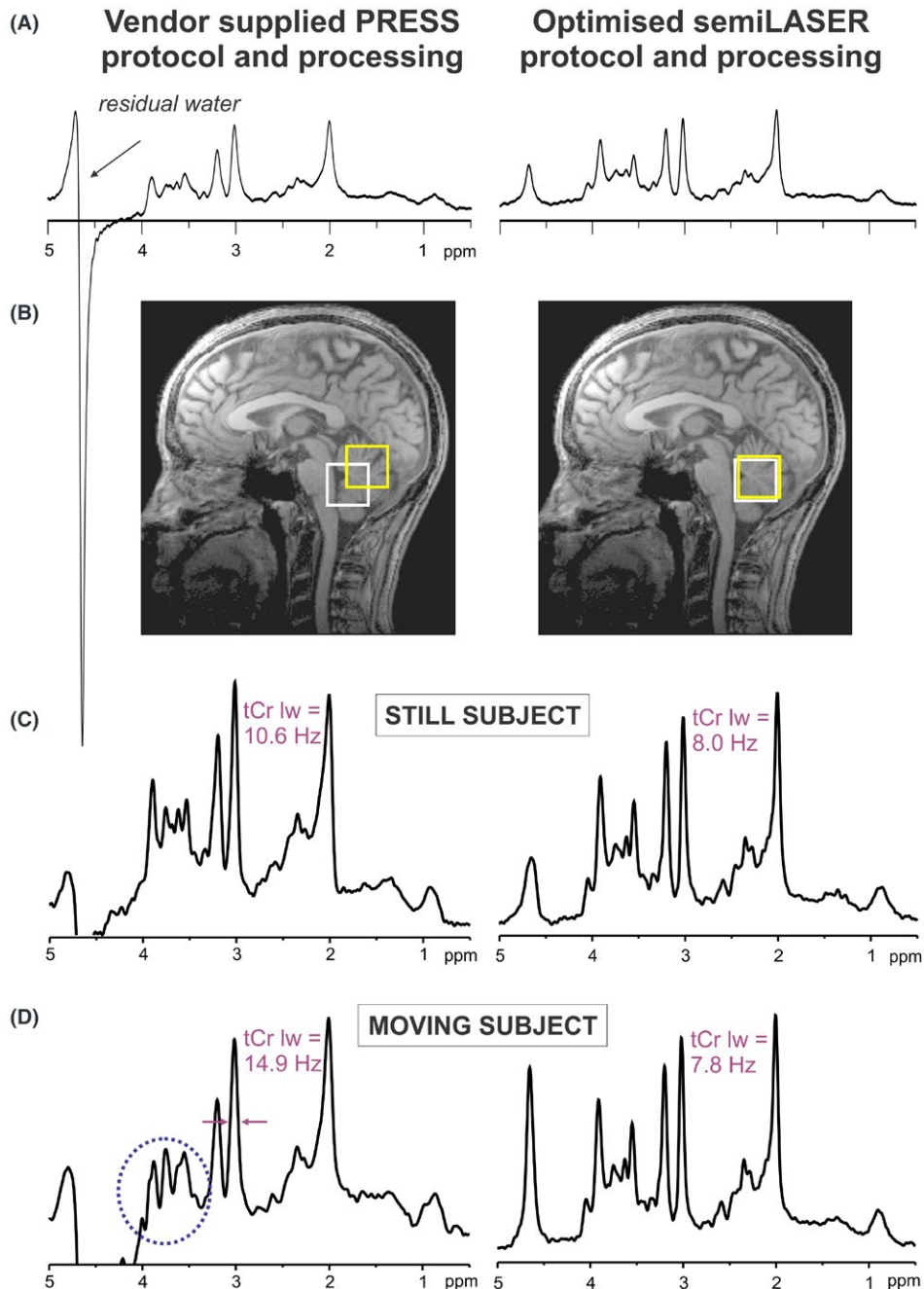


**FIGURE 2** Comparison of vendor-supplied MRS implementation of PRESS versus an advanced in-house protocol using semi-LASER<sup>79</sup> and improved water suppression, shimming, and data processing on a 3T MRI system. Spectra (TE = 30 ms, TR = 5 seconds, 64 transients) were acquired from the same voxel in the cerebellar vermis of a healthy volunteer. A, Water was suppressed by about 150 fold by the chemical shift-selective sequence in the PRESS protocol and about 4500 fold by the variable pulse power and optimized relaxation delays scheme<sup>29</sup> incorporated into the semi-LASER sequence. B, Chemical shift displacement (CSD) for resonances with a chemical shift difference of 3 ppm is 36%-39% with the PRESS sequence versus 6% with the semi-LASER sequence in the 2 dimensions shown. C, Narrower linewidths (shown for the total creatine [tCr] signal) are obtained with FASTMAP shimming<sup>18</sup> in conjunction with single-shot frequency and phase correction in the semi-LASER protocol versus product shimming and signal averaging in the PRESS protocol in the absence of motion during scanning. D, A small amount of motion (few degrees in  $z$  such that the cerebellar volume of interest [VOI] was still acceptable at the extremes of motion) further degrades the linewidths and generates unwanted coherences that are not removed with phase cycling in the PRESS protocol (highlighted by the circle). In contrast, spectral quality is unchanged, with an acceptable water residual in the semi-LASER protocol thanks to artifact-free single shots and frequency and phase correction of individual shots

### 2.1.3 | $B_0$ inhomogeneity

In vivo susceptibility-induced magnetic field distortions arise from the presence of air/tissue and tissue/bone interfaces. In brain, field distortions are most apparent in regions close to sinuses, such as the prefrontal cortex and temporal lobes, and because susceptibility differences scale with the static field strength, these distortions are stronger at higher fields. A homogenous static magnetic field,  $B_0$ , is essential for MRS, as narrow linewidths provide the spectral resolution that is critical for observation of multiplet resonances, accurate metabolite quantification, and efficient water suppression. In addition to gradient coils, MR systems incorporate shim coils to compensate for  $B_0$  inhomogeneity, and adjustment of currents flowing through these coils is called “shimming.”

Vendor-provided shimming routines are currently based on the acquisition of a 3D  $B_0$  field map (GRESHIM),  $B_0$  field mapping along orthogonal projections (FASTMAP and its variants),<sup>18-22</sup> or along orthogonal planes of the localization VOI. The  $B_0$  field variations calculated from signal-phase differences are used to compute the currents needed for each of the available shim coils.<sup>23-25</sup> The  $B_0$  field distortions over typical SVS dimensions are generally compensated using a first-order shim (using the linear  $x$ ,  $y$ , and  $z$  imaging gradient coils) at 1.5 T, whereas the use of second-order shim elements terms ( $z^2$ ,  $x^2-y^2$ ,  $x-y$ ,  $x-z$ , and  $y-z$ ) is strongly recommended for SVS at 3 T.<sup>26</sup>

### 2.1.4 | Water suppression

Detection of millimolar metabolite signals in the presence of 3-4 orders of magnitude higher water (~40 M) signals is challenging due to the spectral baseline interference originating from the tails of the large water resonance. In addition, water “sideband” distortions, originating from various sources including subject movement, as well as mechanical vibration and instability of RF and gradient electronics, produce spurious signals that further confound metabolite signal estimates. Such interferences can be mitigated during acquisition by using a water-suppression module before the MRS localization module. The most common methods exploit the chemical shift difference between water (4.65 ppm) and the strongest metabolite resonances (4.2-0.8 ppm). Common methods include repeated chemical shift-selective saturation pulses at the frequency of water<sup>27</sup>; water suppression enhanced through  $T_1$  effects<sup>28</sup>; and variable pulse power and optimized relaxation delays<sup>29</sup> (Figure 2). In general, the effectiveness of water suppression is significantly affected by  $B_0$  homogeneity, as methods require narrow-bandwidth frequency-selective pulses to avoid inadvertent suppression of metabolite resonances closest to the water resonance.

### 2.1.5 | Voxel dimensions and placement

In nonfocal diffuse brain disease or general physiological studies, the SVS acquisition voxel is preferentially placed far away from air/tissue interfaces, because of shimming difficulties, and away from the scalp to prevent spurious out-of-volume lipid signals. In a 5-minute acquisition time, an 8-cm<sup>3</sup> cuboid volume in parieto-occipital gray matter or parietal white matter provides high-quality spectra at 1.5 T. Smaller volumes down to 4 cm<sup>3</sup> also yield spectra that allow metabolite quantification beyond tNAA, tCr, and total choline (tCho) at 3 T within 5 minutes, provided that good  $B_0$  homogeneity can be achieved. In focal diseases or specific anatomical areas of interest, voxels that best fit the targeted anatomy or lesion are commonly used. Contamination by lipid signals occurs for voxels located too close to the scalp, and trial voxel placement in volunteers to assess slice-profile and CSD limitations experimentally is advised. In addition to careful voxel positioning, outer-volume suppression (OVS) may be used to suppress signal from unwanted regions in challenging areas. In general, volumes below 4 cm<sup>3</sup> do not have an adequate SNR if detailed metabolic profiles are needed to answer clinical questions within a reasonable 5-minute acquisition time, but may be acceptable for restricted analysis such as the tCho/tNAA ratio in brain tumors. Voxel volumes greater than 8 cm<sup>3</sup> or prolonged scan times are needed to detect small changes in low-SNR metabolites such as glutathione, and aid the discrimination between heavily overlapped multiplets such as glutamate and glutamine.

### 2.1.6 | Data analysis

Gross spectral features are amenable to expert visual interpretation (e.g., lipids that indicate a high-grade tumor<sup>30</sup>); however, automated analyses of metabolite signals provide objective measures, such as relative metabolite concentrations or ratios, as biomarkers for clinical decision making and clinical trials.<sup>31</sup> Magnetic resonance spectroscopy analysis using basis sets of known metabolites, MM and lipid signals parametrically fitted to the data with modeling of baseline and peak line-shape variations, have been particularly successful (Figure 1). Fitting may be performed in the frequency domain, where baseline distortions may be modeled as smoothly varying spline functions (LCModel<sup>32</sup>) or decomposed using wavelets (VeSPA<sup>33</sup>). Time-domain analysis may also be used to reduce errors from baseline signals by omitting initial data points from the fit, exploiting the rapid temporal decay of baseline distortions (QUEST<sup>34</sup>, TARQUIN<sup>35</sup>). Metabolite basis sets can be acquired experimentally or simulated from known parameters,<sup>36-38</sup> and either approach is effective.<sup>39,40</sup> The addition of known MM and lipid signals to the basis set results in improved analysis, particularly for short-TE data sets or tumor spectral

analyses.<sup>41</sup>  $B_0$  inhomogeneity and artifacts originating from rapidly changing gradients, known as eddy currents, broaden and distort the MRS line shape from its ideal form (e.g., Lorentzian for singlet peaks). For accurate analyses, these line-shape variations should be reduced by correction based on the unsuppressed tissue water signal<sup>42</sup> and/or modeled during the fitting algorithm.<sup>32</sup>

### 2.1.7 | Data quality

Quality control requires consideration of (1) SNR, (2) metabolite and unsuppressed water resonance linewidths, (3) residual water signal, (4) line shape, (5) Cramér-Rao lower bounds (CRLBs) of the data fit, (6) fit quality (relative size of residuals versus noise SD), and (7) presence of artifacts (spurious signals, baseline distortions, contamination from subcutaneous lipids). The first 6 can be calculated automatically by spectral analysis software; however, the evaluation of artifacts currently necessitates inspection by an experienced reader of MRS.<sup>43</sup> Current automatic quality control suffers from a lack of evidence-based quality thresholds, although general recommendations are available.<sup>1,44,45</sup> An accepted numerical quality estimate in relation to model fitting of MRS data is the CRLB: a lower estimate of the error of the concentration measurement as influenced by SNR, linewidth, and mutual signal overlap. A relative CRLB greater than 50% indicates that there is insufficient information to claim that the estimated value is significantly different from zero; therefore, it is often considered to be unreliable. However, it may also indicate that the estimated value is too low to be reliably measured, which may be clinically significant.<sup>46</sup> Influences from artifacts are not included in the CRLB calculation, and these are illustrated and discussed in Supporting Information Figures S1, S2, and Section B.

### 2.1.8 | Absolute quantitation methodology

The obtained MR signal is proportional to the number of contributing  $^1\text{H}$  nuclei in the VOI, but the signal is not calibrated and measurement of absolute metabolite concentration is challenging due to unknown scaling factors such as receiver coil sensitivity and loading. For metabolite ratios, these factors cancel, and for this reason metabolite ratios (e.g., tNAA/tCr) are widely reported for clinical use, despite the ambiguity of attributing changes to the metabolite in the numerator or denominator. Additionally, small or inaccurate values for the denominator produce large variance in a metabolite ratio. Semiquantitative MRS can be obtained from the ratio of each metabolite to the unsuppressed tissue water signal from the same VOI and using an assumed MR visible tissue water content.<sup>47</sup> Full concentration quantitation requires correction of water and metabolite signals for relaxation factors, assessment of any tissue partial volume effects (e.g., relative

proportions of gray and white matter, CSF, or pathological tissue in the VOI), and correction for disease-induced water concentration alterations.<sup>48</sup> One challenge with concentration measures is that accurate knowledge of water and metabolite relaxation times are required, which may not be available for pathological tissue (see Supporting Information Section C for a discussion on relaxation-time effects on quantitation). In principle, using TEs shorter than 15 ms minimizes absolute quantitation errors of singlet peaks to less than 10% and reduces the dependence on assumed  $T_2$  relaxation values; however, technical challenges with accurate localization at very short TE make this impractical with currently available commercial MRS sequences.

## 2.2 | Magnetic resonance spectroscopic imaging

Although SVS is appropriate for investigation of a focal lesion, a specific anatomical region, or diffuse brain disease, MRSI is preferred when the location of interest is uncertain or multiple areas need to be evaluated simultaneously, such as when investigating metabolite distributions across heterogeneous lesions due to a tumor. In its most commonly used implementation at 3 T, a  $16 \times 16$  grid of spectra with nominal voxel resolution of  $1.5 \text{ cm}^3$  may be acquired in approximately 5 minutes at a TR of 1500 ms, with 1 average per phase-encoding step and elliptical k-space sampling. Despite the advantage of spatial metabolite information offered by 2D and 3D MRSI, robust acquisitions of good-quality data present significant challenges. Practical issues include achieving adequate  $B_0$  homogeneity over a large volume for good spectral resolution and reliable water suppression, good scalp lipid suppression, and automated and accurate analysis of large multivoxel data sets and their presentation for intuitive interpretation. In the following sections, we briefly introduce the technical issues surrounding MRSI acquisition and analysis.

### 2.2.1 | Localization and phase encoding

Contrary to a small voxel that is selected in SVS, in MRSI a larger volume is selected to acquire signals from multiple voxels across a 2D or 3D grid. This volume can be a slice through the brain, acquired using single slice-selective excitation and refocusing pulses combined with OVS slices to suppress scalp lipid. A single 2D slice or 3D cubic volume can be selected with orthogonal slice-localization methods such as PRESS or STEAM as described for SVS. Within the selected slice or volume, 2D or 3D phase encoding is performed to localize spectral signals to a specific grid location. Outer-volume suppression is essential in slice-localized acquisitions to suppress subcutaneous lipid signals, and may be used in combination with PRESS or STEAM localization to reduce spurious outer-volume and scalp lipid signals. The



OVS slices are also used to create a target VOI that better conforms to the brain shape and a relevant tissue region, as well as aid in the optimization of shimming and water suppression over a more restricted region (Figure 3).

Although the CSD, which is expressed as the displacement/ppm as a percentage of the localization width (%CSD), remains constant for a particular sequence, absolute CSD increases proportionally with the prelocalization dimensions. Therefore, increased in-plane CSD is a significant problem for MRSI, in which localization volumes are much larger compared with SVS. Typical 2D MRSI PRESS implementations at 3 T have an in-plane %CSD of over 10%/ppm, resulting in a relative

displacement of 1.2 cm between tCho and tNAA localization volumes for a  $10 \times 10 \times 1 \text{ cm}^3$  axial PRESS volume, in both the left–right and anterior–posterior directions (Figure 4).

The phase-encoding localization method is based on the incremental adjustment of the strength of an applied magnetic gradient field and may be applied to MRS acquisitions to create a “spectroscopic” image.<sup>49,50</sup> Unlike slice localization described previously, localization by phase encoding does not exhibit CSD effects or geometrical distortions due to  $B_0$  inhomogeneity, and allows relative metabolite signal frequencies to be preserved independent of spatial position. Although data matrix sizes are small in MRSI compared with

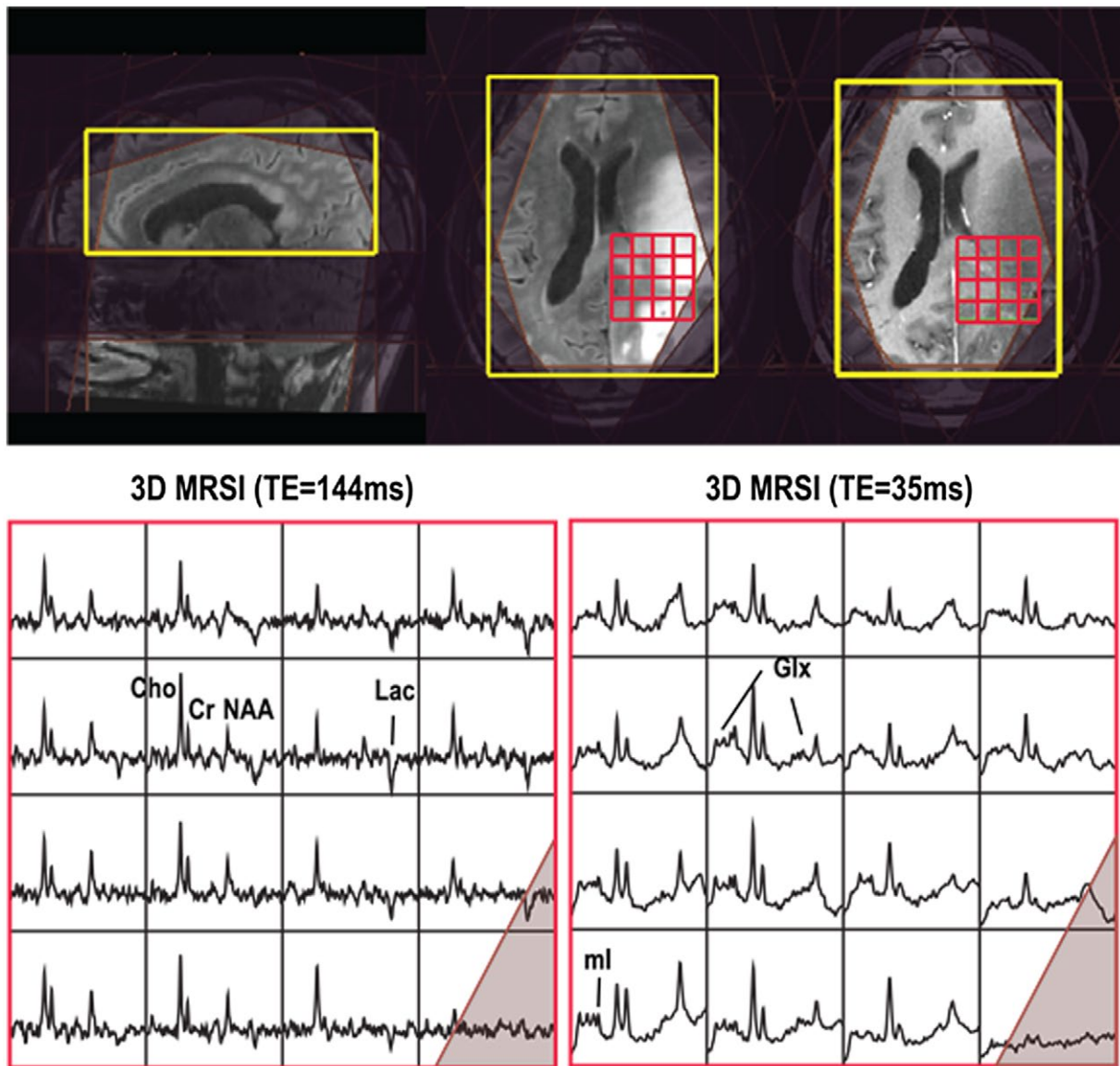


**FIGURE 3** Three-dimensional MRS imaging [MRSI] (bottom left: TE = 144 ms, TR = 1.25 seconds; bottom right: TE = 35 ms, TR = 1.3 seconds) acquired at 3 T from a patient with glioblastoma. Both scans had a nominal voxel resolution of  $1 \text{ cm}^3$ , and 4-Hz spectral apodization was applied. The PRESS excitation volume (yellow rectangle) and 8 very selective saturation (VSS) outer suppression bands (shaded purple) are shown in the top panel. Both the PRESS volume and VSS outer suppression bands were automatically prescribed using in-house software.<sup>107</sup> Good-quality spectra from the red gridded region (top) of slices close to the center of the PRESS box are highlighted for both long and short TEs (bottom)

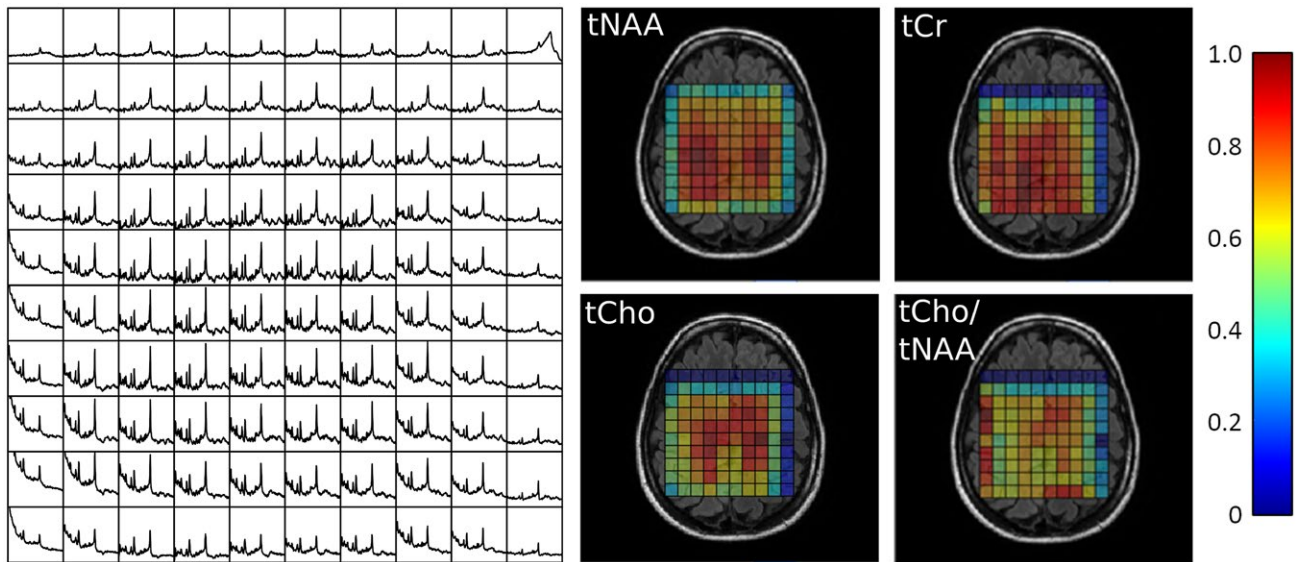


**FIGURE 4** Two-dimensional PRESS CSI acquired at 3 T in a healthy volunteer using TR = 2000 ms, TE = 32 ms, and elliptical sampling from a  $20 \times 20$  k-space grid with nominal voxel size of  $10 \times 10 \times 10 \text{ mm}^3$  and 13-minute acquisition time (including a reduced spatial-resolution water reference for zero-order phasing). Spectral data are shown over the range of 0.5 ppm to 4 ppm for the central  $10 \times 10$  voxels, and the PRESS localization volume was prescribed as the outer edge of the grid with the transmitter frequency set to the expected frequency of the total N-acetylaspartate (tNAA) resonance at 2.01 ppm. Spectra were analyzed with LCModel, and the metabolite maps are shown in a false color scale normalized to a maximum of 1.0. The PRESS volume edge is defined at the zero excitation level (i.e., the lower tNAA signal in all outer voxels). There are much greater reductions in tCho and tCr in the top rows and right columns due to CSD relative to tNAA, which was the metabolite set on-resonance for the PRESS localization. Thus, the absolute signal intensity is modulated by the nonuniformity of the PRESS excitation and further convolved with the CSD effect when metabolite ratios are used

MRI, acquisition times become substantial as spatial resolution increases or if 3D data are required (e.g., > 51 minutes for 3D MRSI when acquiring a full  $16 \times 16 \times 8$  matrix with TR of 1500 ms). To reduce acquisition times, higher frequency spatial components are sacrificed by limiting the k-space acquisition to a spherical or elliptical region, instead of a rectangular one, which reduces measurement time by 25% for 2D and 50% for 3D MRSI.

The MRSI acquisition planning and results are typically displayed as a grid of voxels, in which the nominal voxel dimensions in the phase-encoded directions are determined by the FOV divided by the number of phase-encoding steps. Unlike SVS, in which it can be reasonably assumed that most/almost all signal originates from the prescribed voxel location, MRSI “voxels” may have a significant amount of signal contribution from outside the displayed grid boundaries or nominal voxel volumes. The point-spread function (PSF) describes precisely how the signal from the surrounding area contributes to a location on the MRSI grid. For phase-encoded MRSI, the PSF is a complex *sinc* function; therefore, the signal within a voxel includes positive and negative contributions that decrease with distance from the voxel center (Figure 5A,C). Scalp lipids are particularly prone to producing signals that are localized within the MRSI grid, distant from their true spatial origin (known as signal “bleed”) due to the MRSI PSF. These artifacts can often cause significant spectral distortion

and confound the true estimation of metabolite and lipid levels originating from brain tissue.

### 2.2.2 | Acquisition-based suppression of scalp lipid

Scalp lipid suppression may also be achieved with OVS, frequency-selective saturation, and inversion recovery (IR) methods, either in isolation or in combination with PRESS or STEAM localization. Outer-volume suppression is typically applied using 8 perpendicular planes to the MRSI excitation, arranged in an octagonal pattern around the scalp.<sup>51</sup> Outer-volume suppression maintains target region signals, but is cumbersome to plan and has limited lipid suppression efficiency. The IR approach with a non-frequency-selective adiabatic inversion pulse is relatively insensitive to  $B_1$  inhomogeneity and eliminates the need for careful OVS prescription.<sup>52</sup> A drawback of IR lipid suppression, however, is that  $T_1$  relaxation also occurs for metabolites in the IR period, resulting in unwanted metabolite  $T_1$  weighting and signal loss (approximately 25% at 3 T), which is greater the shorter the metabolite  $T_1$  is. For many neurological disorders, intracerebral lipids are not of interest; hence, global lipid suppression using IR is inconsequential. However, lipid signals in the target volume are important diagnostically for tumors, stroke, and lipid metabolism disorders.

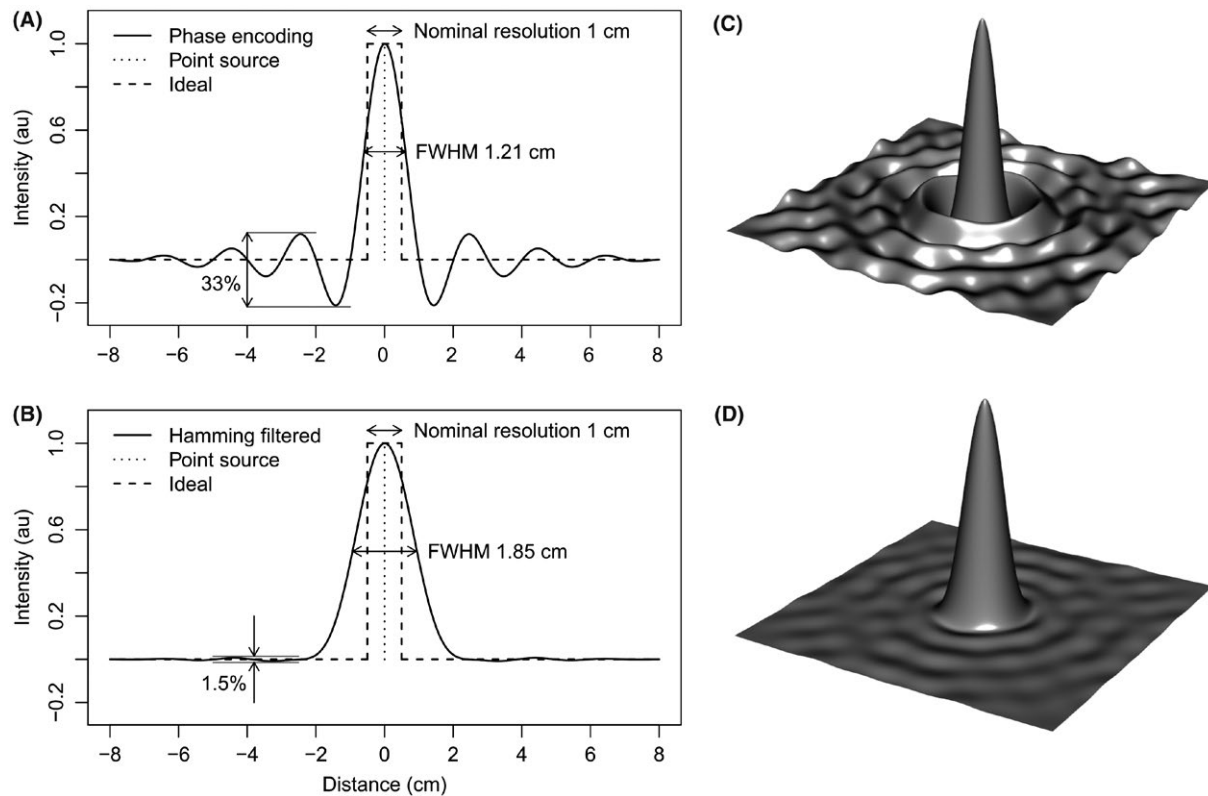


**FIGURE 5** The one-dimensional point spread function (PSF) for phase-encoded MRSI with 16 points (A) and with reduced spatial signal spread and resolution when applying a Hamming k-space filter (B). The PSF of the more commonly used  $16 \times 16$  circularly sampled 2D phase-encoding scheme for MRSI is illustrated in (C) and the corresponding Hamming-filtered PSF is shown in (D). A nominal resolution of 1-cm and 16-cm FOV was used for all plots. Due to the PSF and its filtering, the effective voxel size is considerably larger than the nominal voxel size

### 2.2.3 | $B_0$ inhomogeneity

Adequate shimming is significantly more difficult for MRSI compared with SVS. The  $B_0$  inhomogeneity must be corrected over a larger tissue volume, and  $B_0$  inhomogeneity in regions close to the scalp or sinuses may exacerbate artifacts due to PSF effects. Whole-brain 3D MRSI with first and second-order shimming may have up to 35% of voxels with insufficient data quality for analysis at 3 T.<sup>53</sup>  $B_0$  heterogeneity is so large across the whole brain that the required shim strength for optimal homogeneity increases by an order of magnitude going from a slice above the ventricles to the temporal lobe.<sup>54</sup> Therefore, the need for adequate shimming hardware with second-order shim coils and associated high-power amplifiers, combined with reliable software shimming algorithms, is particularly important for MRSI.

### 2.2.4 | Parallel imaging

For MRSI over large brain volumes, phased-array head coils provide improved sensitivity in cortical brain regions and enable the use of parallel reconstruction methods, such as SENSE, to improve spatial resolution or reduce scan times. Potential artifacts from parallel imaging methods include

incorrectly localized signals, due to the imperfect reconstruction, which may not be visually obvious for metabolites in low-spatial-resolution MRSI data. However, incorrectly localized scalp lipids signals are generally more notable,<sup>55-57</sup> which may be shifted in frequency due to  $B_0$  inhomogeneity and aliased to obscure metabolite peaks. Additional challenges in accurate reconstruction are due to metabolite signals having a considerably lower concentration, and therefore SNR, compared with water. Self-calibration parallel imaging methods, such as GRAPPA, have also been applied to MRSI acquisition.<sup>58</sup> The full impact of parallel imaging methods on MRSI metabolite quantification levels is still under investigation.<sup>53,59,60</sup>

### 2.2.5 | Postprocessing

With multichannel coil acquisitions, corrections for coil-dependent signal strength and phase characteristics for each spectrum must be made to combine the data optimally.<sup>12-14,61</sup> An MRSI scan of the unsuppressed water obtained at low spatial resolution can aid zero-order phasing, frequency offset, and line-shape corrections of the metabolite spectra without a major time penalty. With phased-array coils and SENSE, a water-reference signal for metabolite quantitation



may be acquired at the same spatial resolution as the metabolite scan, but with a significantly reduced scan duration as an alternative to a low-resolution acquisition.<sup>62</sup>

Following recombination of data from the individual coil elements, zero-filling of the k-space data is often used to reduce the apparent voxel size and produce smoother-looking metabolite maps. However, this step only amounts to interpolation and does not reduce the effects of the PSF or increase spatial resolution. Spatial filtering is often applied to reduce Gibbs ringing artifacts from scalp lipid and from truncation artifacts associated with reduced k-space acquisitions.<sup>63</sup> This also causes widening of the central lobe of the PSF, resulting in improved spectral SNR, but reduced spatial resolution. Figure 5 illustrates the influence of the commonly used Hamming filter on the PSF for typical MRSI acquisition parameters. Subsequent to processing the MRSI data in k-space, 2D or 3D spatial Fourier transformation is applied to generate a series of FIDs for each voxel. These may be analyzed in the time or frequency domain with the same methods used for SVS, or simply Fourier transformed in the chemical shift dimension to create an array of spectra for a visual assessment.

### 2.2.6 | Data analysis and metabolite maps

Two-dimensional and 3D MRSI produce large amounts of data; therefore, robust, automated data processing to generate metabolite maps is needed for ease of clinical interpretation. Acquisitions at 3 T with phased-array head coils have greater spatial variation in receive sensitivity than studies at 1.5 T with quadrature or birdcage head coil designs, and at 3 T dielectric effects can compromise RF transmission homogeneity. Hence, using a semiquantitative approach with reference to contralateral brain or a coil reference sample are problematic. The MRSI metabolite concentrations can be calculated if an additional water reference is acquired<sup>48</sup>; however, the associated time penalty may be significant (when using conventional methods), as all phase-encoding steps need to be repeated. Metabolite ratio maps can be more robust than maps of “absolute” levels (albeit semiquantitative if relaxation effects are ignored), as they are less sensitive to tissue partial-volume effects with CSF. However, partial-volume effects between tissue types such as gray and white matter,<sup>64,65</sup> or normal and diseased tissues,<sup>66</sup> are important to consider when interpreting the data.

### 2.2.7 | Cautions and quality control

Automatically generated metabolite maps can be unreliable due to the effects of poor water suppression, lipid contamination and  $B_0$  inhomogeneity, and they are degraded by subject motion and inaccuracies of spectral fitting. Therefore, quality assessment of individual spectra and their fit is a required

step for proper interpretation. However, visual quality assessment is often impractical with MRSI, resulting in a need for automated methods to exclude poor-quality data. The relative CRLB derived from fitting each spectrum to a model function is misleading as a numeric estimate of data quality if there is a real absence of specific metabolites; however, good CRLB values may also arise from fitting bad-quality spectra if the noise is underestimated, artifacts are present, or the fitting method has converged to an incorrect solution (local minimum). Alternative quality measures include CRLB values from a fit to a co-located water signal, using confidence limits<sup>67</sup> and linewidths from spectral fitting of metabolites or water, detection of outlying values in the spectrum,<sup>68</sup> and use of pattern recognition to classify poor-quality spectra.<sup>44,69,70</sup> A quality map enables easy interpretation at the time of the clinical read, such as implemented in the MIDAS software<sup>71</sup> (Figure 6). Nevertheless, a visual assessment of spectra in key diagnostic locations is still advisable, and a zoomed-in grid of the raw spectra overlaid on the MRI of the abnormal region adds confidence to any interpretation of metabolite maps.

In addition to poor-quality data, visual interpretation of metabolite maps can present difficulties, particularly at the low spatial resolution of MRSI as compared with MRI, for which partial-volume effects can be significant. Highly interpolated MRSI data can give a misleading impression of spatial detail, and PSF effects reduce the actual spatial resolution and may create artifactual “hot” or “cold” spots.  $B_0$  inhomogeneity can cause localized signal loss, which may be obvious in temporal-frontal brain regions due to proximity to sinuses, but can also occur in areas of blood breakdown products or calcification, and close to surgical entry points (e.g., craniotomy staples). Finally, maps of metabolite ratios can include exceptionally high values because of a division by a small metabolite value, and visual inspection is required to interpret these regions correctly.

## 3 | CONSENSUS OPINION AND RECOMMENDATIONS

The following discussion is based on the results of an MRS technical consensus survey completed by 35 experts in clinical MRS (Supporting Information Section A) and subsequent discussions among all authors. The survey aimed to determine what specifically could be recommended as best practice using the current standard implementations of  $^1\text{H}$  MRS, and to define current limitations of scanner hardware and software. The survey also indicated the practical solutions that have been developed within the research environment. Key areas inhibiting the more widespread clinical use of MRS are limitations in shimming algorithms, the practicalities of voxel planning and the time penalties associated

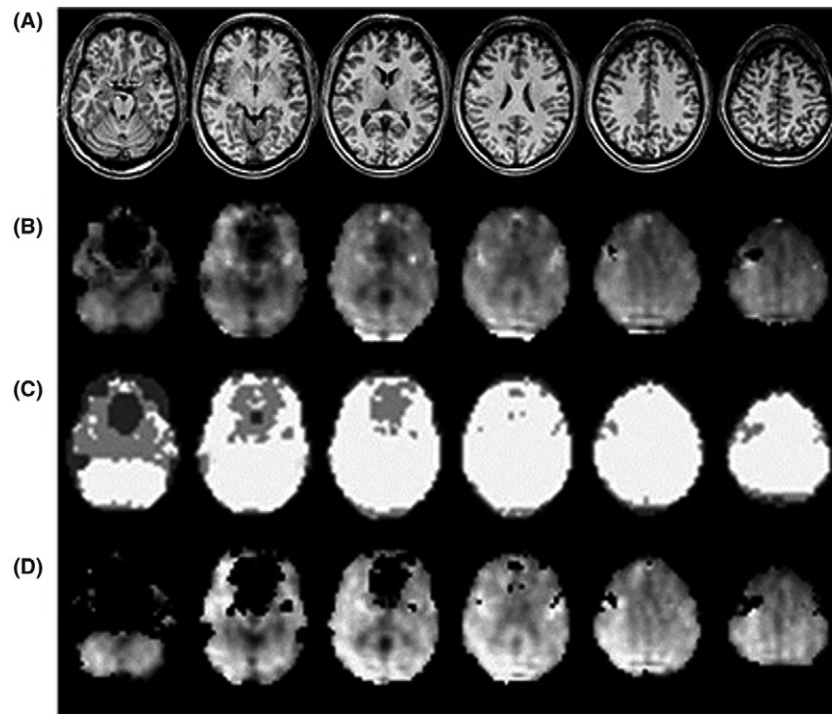


**FIGURE 6** Illustration of spectral quality maps generated by the MIDAS software package.<sup>71</sup> A, T<sub>1</sub>-weighted MRI corresponding to the selected MRSI slices. B, Raw tNAA signal intensity map. C, Spectral quality map, showing regions that passed the quality criteria for metabolite linewidth of 0.1 ppm or less (white). Regions that failed metabolite linewidth-quality criteria, but passed water-reference linewidth criteria, are shown in light gray. Regions that failed both linewidth criteria are shown in dark gray. C, The tNAA map with the identified poor-quality voxels set to zero. Note the signal dropout in much of the anterior cingulate cortex, related to insufficient shimming close to air–tissue interfaces (e.g., sinuses, ear canals). Data were obtained using volumetric (3D echo planar spectroscopic imaging [EPSI]) proton (<sup>1</sup>H) MRSI with lipid inversion nulling at 3 T, TE/TR/TI = 17.6/1550/198 ms, 50 × 50 × 18 k-space points over 280 × 280 × 180 mm<sup>3</sup>, and total acquisition duration of 16 minutes

with these processes, as well as reliable data processing and display. All of these issues are significantly exacerbated for MRSI. We indicate solutions to these issues and provide guidance for recommended acquisition and data-processing protocols within the context of current scanner capabilities.

### 3.1 | Single-voxel spectroscopy acquisition

Point-resolved spectroscopy localization is the current standard for SVS and is commercially available from all scanner manufacturers. We recommend a maximum CSD level of 4%/ppm, in which the percentage relates to the spatial displacement as a proportion of the slice-selection width. This maximum recommended level of CSD is achieved at 1.5 T, but exceeded in some implementations at 3 T due to insufficient bandwidth of conventional RF pulses resulting from a limited maximum transmit field  $B_{1max}$ . Increased CSD makes planning and interpretation of SVS more challenging due to different metabolite signals being localized to different volumes. Therefore, methods to reduce CSD, while maintaining good SNR, short TEs and accurate localization, should be used to achieve the full advantages of clinical MRS at 3 T. One of the first approaches to reduce CSD was the use of very selective

saturation (VSS) pulses that have high bandwidth and can suppress an outer-volume signal with minimal CSD. Conventional PRESS is used to excite a larger (approximately 20%) region than required, and VSS pulses redefine a smaller region with minimal CSD,<sup>72,73</sup> a method known as OVERPRESS.

Adiabatic pulses have a substantially greater bandwidth (for a given  $B_{1max}$ ) than the conventional refocusing pulses used in the PRESS sequence and were first applied to 3D, single shot localized MRS in the SADLOVE sequence,<sup>74,75</sup> and later employed in the closely related LASER sequence.<sup>76</sup> More recently, the semi-LASER<sup>77-79</sup> sequence has been developed, replacing the adiabatic excitation pulse of LASER with 1 conventional slice-selective excitation pulse to reduce the minimum achievable TE. Higher-order hyperbolic secant adiabatic full passage or gradient-modulated offset-independent adiabaticity pulses may be used for refocusing in semi-LASER, with the latter using wideband, uniform rate and smooth truncation RF and gradient waveform modulation.<sup>80,81</sup> The advantage of gradient-modulated offset-independent adiabaticity pulses compared with hyperbolic secant adiabatic full passage is a reduced maximum  $B_1$  strength required for a given pulse bandwidth, enabling semi-LASER to be used at short TE (~30 ms) on 3T systems with a maximum available



$B_1$  strength of 13–15  $\mu\text{T}$ .<sup>82</sup> In addition, gradient-modulated offset-independent adiabaticity semi-LASER has a reduced RF power deposition compared with hyperbolic secant adiabatic full-passage pulses of the same bandwidth, enabling the sequence to be used with a shorter TR and at higher field strengths within specific absorption rate limits. Although adiabatic pulse pairs offer improved resilience to  $B_1$  inhomogeneity, their primary advantage for SVS at 3 T is increased bandwidth and slice-selection profiles, thereby reducing CSD to acceptable levels. A further advantage of semi-LASER, compared with PRESS for the same TE, is longer apparent  $T_2$  relaxation times and partially suppressed  $J$ -coupling evolution, due to the Carr-Purcell-Meiboom-Gill-like refocusing pulse train (and therefore enhanced detection of complex multiplets such as glutamate.)<sup>79,83</sup>

Overall, we recommend the use of semi-LASER due to its recent validation studies<sup>84–89</sup> and increasing availability on clinical systems, as both research work-in-progress sequences and commercial product (Figure 2). Furthermore, in our consensus survey, semi-LASER was ranked as the most likely localization technique to improve clinical MRS. We also recommend the use of PRESS with VSS pulses if this is the only option available, but note this option lacks the partially suppressed  $J$ -coupling evolution and longer apparent  $T_2$  relaxation when compared with semi-LASER, and can inadvertently excite or refocus large signals (e.g., scalp lipids) that are difficult to suppress fully.

In general, we recommend the shortest achievable TE for SVS at any field strength, assuming that CSD remains within the

acceptable range of 4%/ppm and appropriate analysis methods are used to model the increased amplitude of macromolecular and lipid signals. The advantages of using the shortest possible TE include (1) improved SNR due to reduced  $T_2$  relaxation, (2) more accurate concentration estimation due to a reduced dependence on assumed metabolite  $T_2$  values, and (3) improved SNR for  $J$ -coupled metabolite signals due to reduced dephasing. Other TEs may be appropriate for improved detection of specific metabolites, such as lactate/alanine at a TE of 144 ms or TE of 97 ms for 2-hydroxyglutarate with PRESS.<sup>90</sup> Longer TEs may also be preferred to improve water and lipid suppression, due to their shorter  $T_2$  compared with metabolites, or if optimal long TE biomarkers are targeted, such as tCho/tCr in glial tumor grading.<sup>91</sup> A SVS TR of 1.5 seconds at 1.5 T and 2.0 seconds at 3 T is recommended to provide the maximum SNR per unit time, on average, for the main metabolite signals from tCho, tCr, tNAA, and lactate. Further justification and discussion on the compromise among TR, SNR, and  $T_1$  saturation may be found in Supporting Information Figures S3, S4, and Section C).

The recommended number of averages for typical voxel dimensions of  $15 \times 15 \times 15 \text{ mm}^3$  and  $20 \times 20 \times 20 \text{ mm}^3$  for 1.5 T and 3 T are given in Table 1. A reduction in voxel dimensions results in a loss of SNR; therefore, additional averages are required to attain suitable quality data. Note that SNR scales with the square root of the number of averages. Accordingly, an unacceptably long time is required for the 15-mm-sided cubic voxels to attain the same SNR as with the 20-mm-sided cubic voxels; therefore, the recommended averages represent a compromise that results in an SNR reduction

**TABLE 1** SVS acquisition consensus summary

Aspect	Consensus
Localization method	CSD of less than 4% per ppm. 3 T: Semi-LASER with OVS (preferred) or OVERPRESS with VSS. 1.5 T: Semi-LASER with OVS (preferred) or PRESS.
TE and TR	TE as short as possible (typically 30 ms). Longer TEs may be preferred for lactate (144 ms or 288 ms) at TEs optimized for specific metabolites, such as 2HG detection, and for enhanced lipid suppression. TR = 1.5 seconds at 1.5 T, 2.0 seconds at 3 T.
Number of averages, voxel dimensions, and sampling parameters	128 averages collected from a $15 \times 15 \times 15 \text{ mm}^3$ VOI at 3 T. 64 averages from a $20 \times 20 \times 20 \text{ mm}^3$ VOI at 3 T. 256 averages collected from a $15 \times 15 \times 15 \text{ mm}^3$ VOI at 1.5 T. 128 averages from a $20 \times 20 \times 20 \text{ mm}^3$ VOI at 1.5 T. Spectral sampling of 1024 complex data points from 2000-Hz spectral width at 1.5 T or 3 T.
Water-reference acquisition	Recommended in all cases. Collect with the same sequence parameters as the water-suppressed scan, but without water suppression and the transmitter frequency set to the water resonance. A single average should be collected with a pre-acquisition delay time of at least 9 seconds to prevent $T_1$ weighting
$B_0$ shimming hardware	Second-order shim coils with adequately powered amplifiers are recommended at 3 T.
$B_0$ shimming algorithm	Methods incorporating shim-strength limits and instability countermeasures are preferred over unconstrained approaches.

Abbreviations: 2HG, 2-hydroxyglutarate; OVS, outer-volume suppression.

of 40% for the smaller voxel size. However, because shimming is generally improved for smaller voxel sizes, some signal loss is mitigated by narrower linewidths.

In addition to water-suppressed data, which are required for metabolite level/concentration estimation, a matched unsuppressed water-reference acquisition (acquired with the transmit frequency set to the water resonance) is recommended as part of all SVS clinical protocols. Because the water resonance has high SNR compared with metabolites, we recommend acquiring a single average for the water-suppressed data. When possible, a minimum period of 9 seconds without RF excitation should be ensured before acquisition, to essentially eliminate  $T_1$  weighting for water in normal and pathological tissue. A 9-second delay also ensures that the  $T_1$  saturation signal loss is less than 10% in cystic regions or CSF. Dummy scans should be used to achieve a steady state in cases in which the recommended relaxation period cannot be guaranteed. The water signal may be used to correct for eddy current line-shape distortions<sup>42</sup>; estimate  $B_0$  field homogeneity and frequency offset; evaluate water-suppression quality; and provide metabolite concentration scaling information for use with short TE acquisitions.<sup>47</sup>

### 3.2 | Magnetic resonance spectroscopy imaging acquisition

The MRSI acquisitions excite a much larger volume of tissue compared with SVS; therefore, a more stringent maximum CSD of 2% per ppm (across the selected volume) is recommended. Any CSD levels greater than 2% per ppm result in a significant loss of metabolite information around the edges of the MRSI excitation region, making it challenging to obtain the required spatial coverage in the cortex, such as avoiding unwanted excitation of scalp lipids. It is recommended that edge voxels be excluded from the from data analysis. We recommend the use of semi-LASER over PRESS for 3T MRSI prelocalization, due to its reduced CSD level and additional reasons stated in the SVS acquisition section. Where available, the use of high-bandwidth spatially selective saturation bands<sup>92,93</sup> are also recommended to improve conformance between the excitation volume and the region of interest by suppressing scalp lipid regions that are unavoidably excited by the prelocalization scheme. Standard OVS is also recommended for suppressing signals from brain areas with significant  $B_0$  inhomogeneity (e.g., frontal sinuses), to reduce PSF-related distortion spread. A narrower PSF, resulting from acquisition with higher in-plane resolution, is also recognized as an effective strategy for reducing scalp lipid contamination—provided that the extra scan time and reduced SNR can be tolerated.

For 2D phase-encoded MRSI, we recommend the use of elliptical sampling in k-space and TRs of 1.5 seconds at 1.5

T and 2.0 seconds at 3 T (Supporting Information Section C). The phase-encoding FOV should fully encompass the prelocalization volume to avoid aliasing, and the use of a  $16 \times 16$  imaging matrix with 10-mm in-plane resolution and slice thickness of 15 mm is recommended as a default protocol. Note that the recommended spatial coverage and resolution parameters are intended as a starting point only, and may need to be adjusted to match the disease location, extent, and clinical question. For instance, in the case of inadequate prelocalization, the phase-encoding FOV should be increased to contain regions of spurious signals to avoid aliasing. As with SVS, short TEs (approximately 30 ms) are recommended for MRSI, due to the greater level of metabolite information, higher SNR, and reduced  $T_2$  bias in concentration estimates. However, in areas of greater  $B_0$  inhomogeneity, where water and lipid suppression are less effective, longer TEs may be necessary to reduce water and lipid signals relative to metabolites. An unsuppressed MRSI water scan should be acquired to aid line-shape correction, phasing, chemical-shift referencing, and quantitation. Because an additional MRSI water acquisition doubles the effective scan time for MRSI at the same spatial resolution (unlike SVS), a reduced resolution acquisition or parallel imaging<sup>62</sup> approach may be used to mitigate the associated time penalty for acquiring the unsuppressed water MRSI.

Although 2D phase-encoded MRSI with prelocalization is currently the most commonly used MRSI technique in the clinical environment, there is strong interest in the development of robust whole-brain MRSI within a clinically feasible acquisition time. In addition to the obvious advantages for studying diseases that are known to affect multiple brain areas, such as neurodegeneration,<sup>94</sup> the ability to plan an MRSI acquisition as easily as standard MRI (i.e., without having to preselect a region of interest) will improve data consistency and acceptance in clinical centers. The use of prelocalization also significantly restricts spatial coverage, making it very difficult to study cortical regions near to the surface of the brain. Using conventional phase encoding, 3D MRSI is only practical for limited brain regions when there is the option of highly efficient OVS. For instance, the use of VSS pulses<sup>73</sup> or a 3D  $8 \times 8 \times 8$  MRSI matrix of 15-mm isotropic voxels provides good quality data in 12.8 minutes for a TR of 1500 ms and a full k-space acquisition. For whole-brain examination, 3D MRSI is prohibitively time-consuming; therefore, a number of fast acquisition methods have been developed by the research community.

The most commonly used whole-brain MRSI acquisition is the echo planar spectroscopic imaging (EPSI) technique,<sup>95-97</sup> in which an oscillating readout gradient generates an echo train, encoding a full plane of k-space for each excitation. When applied to the proton nucleus, PEPSI (proton PEPSI) is also used to describe the same sequence<sup>98</sup>; however, we generally recommend the use of the more generic term EPSI.

The chemical shift and 1 spatial dimension are simultaneously encoded during the gradient-echo readout, and phase encoding is used for the 2 remaining spatial dimensions. Recent implementations of EPSI use either whole-slice/slab acquisition with OVS<sup>99,100</sup> or whole-brain acquisition with lipid inversion nulling and postacquisition k-space extrapolation<sup>101</sup> to significantly reduce scalp lipid contamination. In addition, an interleaved water acquisition is used to improve reconstruction in the presence of  $B_0$  inhomogeneity and drift, and to provide a reference signal for metabolite concentration scaling.<sup>102</sup> Unlike many other MRSI approaches, the whole-brain 3D EPSI sequence has been implemented and tested on instruments from 3 manufacturers with encouraging consistency across sites.<sup>103</sup> The main advantages of this sequence are greater coverage of the cerebrum and simpler planning. This sequence has been reported to sample, on average, 70% of the brain volume,<sup>104</sup> although with instrumentation-dependent differences. Recent 3T studies using whole-brain 3D EPSI have been able to achieve an acquisition time of 18 minutes with a TE of 20 ms, which may be acceptable for clinical trials and some specialized clinical assessments.<sup>105</sup> Shorter scan times are feasible using partial-brain 3D EPSI.<sup>100,106</sup>

An alternative approach for whole-brain MRSI is to combine medium-resolution EPSI encoding (10-mm isotropic) with OVERPRESS localization and automatically prescribed VSS bands.<sup>107</sup> This sequence is relatively fast to acquire (13 minutes) and does not require lipid inversion nulling, which also suppresses potentially useful lipid signals originating from pathology. In addition, the automated prescription of this sequence is much more practical for clinical use when compared with manually prescribing PRESS volumes in combination with saturation pulses and shim volumes. This approach has been tested on a clinical cohort of brain tumor patients with encouraging results.<sup>107</sup>

Considerable progress toward robust whole-brain MRSI has been made in recent years, and a wide range of techniques has been demonstrated to provide high acceleration.<sup>106,108</sup> At the time of writing, we were unable to recommend one whole-brain MRSI approach over another, and identified a need for comparative studies to assess the relative performance of the various approaches.

### 3.3 | Single-voxel spectroscopy and MRSI preprocessing and analysis

Fully automated analysis methods, which perform phase correction, chemical shift calibration and quantitative analysis of metabolite signals, have been available for 25 years<sup>32</sup> and are strongly recommended for MRS analysis. A choice of commercially licensed (LCModel<sup>32</sup>), free (jMRUI<sup>109</sup>), and open-source (e.g., TARQUIN,<sup>35</sup> MIDAS,<sup>71</sup> SIVIC,<sup>110</sup> VeSPA [<http://scion.duhs.duke.edu/vespa/>]) software packages have been developed, predominantly by the research community, and are

available for offline data visualization and analysis. Analysis methods available on the scanner software are typically inferior to those used in dedicated software packages, and an improvement in this area would greatly benefit clinical MRS. There is currently no clear consensus on the best analysis algorithm for use in all cases; however, a common feature of the most widely used methods is the use of a quantum mechanically simulated set of metabolite spectra (basis set) into the fitting routine. Modeled lipid signals and modeled or measured macromolecular signals can be included in the basis set when appropriate (e.g., short TE protocols or investigations of pathologies with hypoxic/necrotic processes such as stroke and tumors).

The jMRUI, TARQUIN, and VeSPA packages have metabolite basis simulation integrated into the analysis software. In the case of jMRUI, metabolite simulation is performed using the NMRSCOPE-B<sup>111</sup> method and VeSPA makes use of the GAMMA library.<sup>112</sup> The FID-A package also provides tools to simulate metabolite basis sets, in addition to preprocessing steps and data export options for fitting to be performed with other software.<sup>113</sup> We recommend the use of analysis methods based on fitting with simulated metabolite basis sets over single-peak modeling or spectral integration, as simulated basis sets conveniently incorporate a greater level of prior knowledge<sup>38,41</sup> into the fitting process, which can easily be adapted to match the acquisition protocol.

Quality assessment must be an integral part of MRS analyses, as distorted or poorly fit data leads directly to erroneous results. Metabolite SNR and linewidth estimates are recommended as objective measures of data quality. A number of spectral SNR definitions have been described for MRS. Here, we recommend that the signal measure be defined as the height of the largest metabolite data point in the real part of the spectrum minus the fitted baseline at that point; and the noise measure as 2 times the SD of the spectral data points in a region free from metabolite signals, residual water, or other spectral distortions. Although other measures of spectral SNR are acceptable, reported values should be accompanied by a definition to avoid ambiguity; for example, the current version of the LCModel<sup>32</sup> analysis package defines the noise as 2 times the SD of the fit residual. Linewidth estimates (FWHM) are also usually measured, in units of hertz or parts per million, from the real part of the phased spectrum and are typically derived from the most prominent singlet metabolite or unsuppressed water resonance. Although universal guidelines for acceptable MRS data quality are challenging, due to the heterogeneous metabolite profiles of diseases and wide range of acquisition protocols, spectra with FWHM greater than 0.1 ppm should be regarded as being of poor quality. A minimum metabolite SNR of 3 is recommended to confirm the presence of a particular singlet; however, greater metabolite SNR values are required for accurate quantification or detection of coupled multiplets. Sample spectra with different SNR and FWHM values are shown in Figure 7.

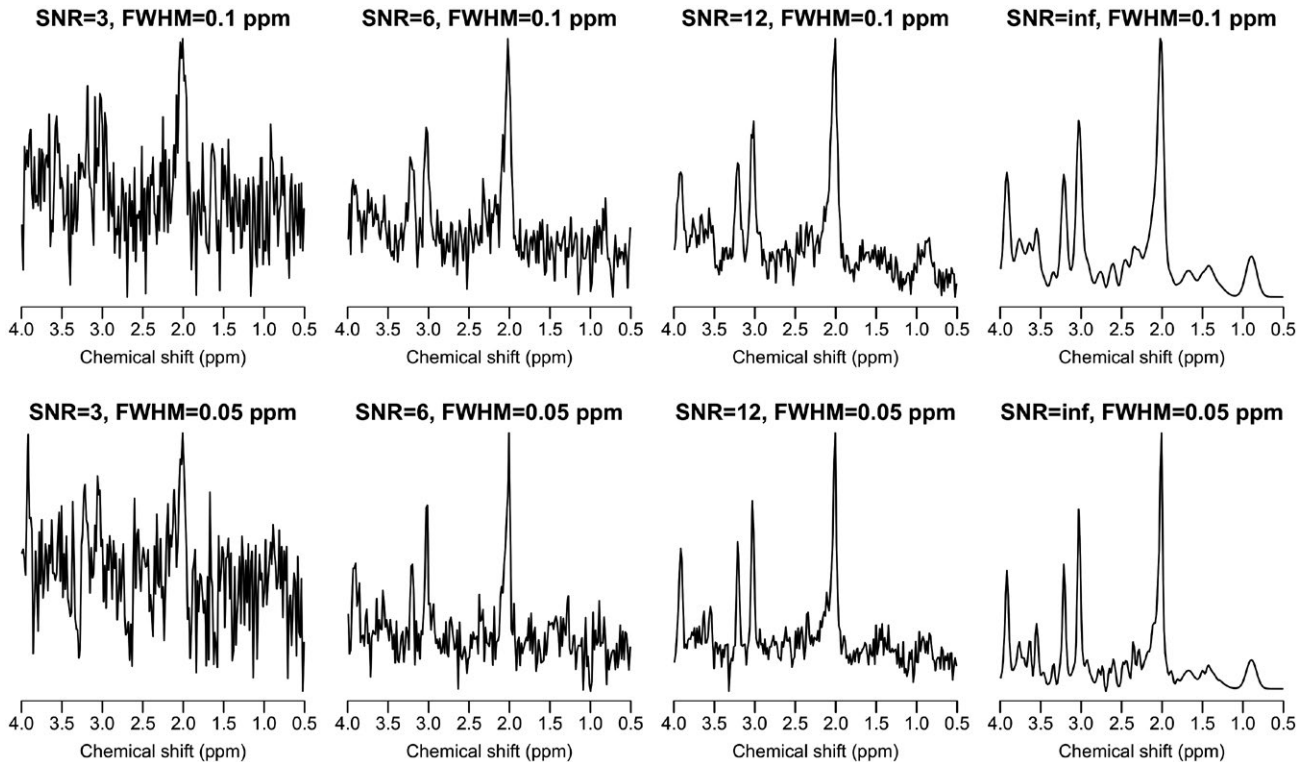


**FIGURE 7** Simulated “normal brain” spectra for a typical PRESS acquisition at 3 T (TE = 30 ms, 1024 data points, and 2000-Hz sampling frequency). The SNR and FWHM values are given for the largest singlet resonance (tNAA)

Although SNR and linewidth criteria are useful for basic quality assessment, a visual inspection of fitting results remains important, as analysis errors and data artifacts may produce unrealistic values. Furthermore, these values do not reliably detect a number of quality issues such as unstable or unrealistic baseline estimates during fitting or out-of-volume lipid contamination. To aid visual assessment, we recommend that the analysis output include plots of the phased spectra with the fit and estimated baseline and residual for retrospective visual assessment of the data (example given in Figure 1 with the optional addition of individual basis signals). For SVS, a quick visual assessment of the data and fit quality can easily be performed by someone with a basic understanding of MRS and common artifacts,<sup>43</sup> and this approach is suitable for the clinical environment. However, for MRSI, where hundreds of spectra are typically acquired in a single scan, visual assessment is often impractical and there is great interest in developing automated quality assessment. One of the first approaches, based on the classification of independent spectral components, was found to provide 87% agreement with expert spectroscopic evaluations.<sup>70</sup> More recently, methods based on random forest classification of spectral data<sup>69</sup> and features extracted from the time and frequency domain<sup>114</sup> have also been shown to provide high agreement with expert assessment. Although these techniques are an important step toward fully automated MRS quality control, their applicability across different scanners, experimental protocols, and clinical scenarios requires further investigation.

Before SVS fitting, eddy-current correction using the unsuppressed water reference is recommended to reduce metabolite signal line-shape distortions.<sup>42</sup> There is also an increasing trend toward retrospective frequency and phase correction of each average and elimination of motion-corrupted FIDs prior to signal averaging.<sup>115-117</sup> Although these methods have been successfully applied to scans with high metabolite signal (e.g., normal appearing brain), their suitability for low-SNR clinical spectra (e.g., brain tumors) has not been fully investigated and therefore should be used with caution. We also note the promising approach of using “metabolite-cycled” MRS for retrospective correction using the water signal, allowing low-SNR spectra to be accurately corrected, while maintaining metabolite spectral quality.<sup>118</sup>

The analysis pipeline for MRSI includes preprocessing steps to aid interpretation. K-space filtering with a suitable window function, such as Hamming, is recommended for reducing distortions from Gibbs ringing of high-intensity signals such as scalp lipids. Fourier interpolation, by k-space zero filling, to twice the acquired dimensions is also recommended to aid display and interpretation of metabolite maps. Optimized reconstruction methods, such as the Papoulis-Gerchberg algorithm, are also recommended to reduce lipid artifacts.<sup>101</sup> More recently, a variety of novel reconstruction methods were shown to suppress MRSI lipid signals<sup>119-122</sup> with promising initial results, but



validation on clinical data is required before recommending them for general use.

### 3.4 | $B_0$ inhomogeneity and water suppression

The current generation of commercially available shimming and water-suppression algorithms does not provide the reliability and robustness needed for performing MRS/MRSI at all locations in the brain. In addition to being quite time-consuming, these drawbacks are important impediments to the wider clinical use of MRS. Therefore, we encourage the research community and MR vendors to optimize the performance of shimming, water suppression, and power-calibration steps in both favorable and challenging brain regions.

Both projection (FASTMAP and variants) and volumetric mapping acquisition methods are widely available, and can be effective for  $B_0$  shimming, with projection methods generally taking less time. A recent study demonstrated that FASTMAP linewidths were 40% better than a vendor implementation of volumetric mapping for an 8-mL SVS VOI in the posterior cingulate cortex.<sup>85</sup> We note that the vendor implementation of volumetric mapping has since been updated and improved, highlighting the challenges of comparing shimming methodology: Seemingly minor implementation differences often have a significant effect on the overall performance of a particular strategy.

Although volumetric mapping methods are thought to be better suited for large VOIs typical to MRSI, no systematic studies have been published by the time of this writing that test this assertion. In addition to the  $B_0$  mapping strategy, the shimming optimization method is crucial for automated and reliable shimming, and a number of algorithms have been published and recently compared.<sup>123</sup> Improved performance was found for methods incorporating known constraints on the maximum available shim strengths and mitigation for instability; therefore, these types of methods are recommended over simpler unconstrained algorithms.

Adequate hardware is essential for good  $B_0$  homogeneity, and second-order shim coils are recommended for MRS of acceptable quality, particularly at 3 T. In addition, adequately powered shim amplifiers are important to ensure good-quality data in anatomic regions such as the hippocampus and frontal brain regions, where there are large susceptibility gradients.

Our recommendations for second-order shimming hardware, combined with accurate  $B_0$  field mapping and robust shimming optimization methods, enable the acquisition of SVS with acceptable spectral quality throughout the brain at 3 T. However, for whole-brain MRSI techniques, such as 3D EPSI, the requirement for homogeneous  $B_0$  across all brain regions simultaneously cannot be achieved with second-order shim coils. Figure 6 illustrates how poor  $B_0$

homogeneity results in unusable spectra in the anterior cingulate cortex when using 3D EPSI, therefore restricting the use of MRS in this region to 2D MRSI or SVS techniques. Homogeneous  $B_0$  across the whole brain is also desirable for gradient-echo EPI, and particularly challenging at ultrahigh field (7 T and above), resulting in the development of a number of novel shimming approaches.<sup>124,125</sup> Although these methods show great potential for improving MRS, at both low and high field, it is currently unclear which will provide the best balance among patient comfort, cost, and efficacy.

### 3.5 | Data formats and interoperability

The MRS results and data may be exported from the scanner console in the following formats: (1) DICOM MRS, (2) DICOM secondary capture, and (3) data points stored in a proprietary format. The DICOM secondary captures (or “screenshots”) typically store an image of the spectrum and fit, alongside the voxel location and quantitative measures, such as metabolite ratios. For MRSI, metabolite maps are also generally displayed together with relevant MRI scans. Although secondary captures are essential for rapid clinical interpretation, they do not allow re-analysis or interactive inspection of the data, which is particularly important for MRSI. For example, following an initial analysis, it may become clear that a brain region has an abnormal metabolite profile that is consistent with a brain tumor; therefore, a re-analysis is required using a cancer-specific metabolite ratio map with a basis set containing additional metabolites, or it may be advisable to re-inspect the spectral quality in crucial areas.

Storage of the acquired complex MRS data points, either in the time or frequency domain, is essential to ensure the extraction of maximal information. Historically, each vendor had 1 or more proprietary formats for exporting raw data files—primarily for offline analysis with third-party tools such as LCMoel.<sup>32</sup> However, proprietary formats have the following disadvantages: (1) They require extra time and computing resources to generate and securely archive, particularly when a hospital contains multiple scanners from different vendors; (2) patient details may not be stored in a way that allows the reliable identification of files, creating problems for comparing scans obtained from multiple sites/scanners and effective de-identification—often a requirement for clinical trials; and (3) additional burden is placed on researchers and third-party software developers to support the file formats, which often change with software updates.

To address these issues, the DICOM standards committee introduced Supplement 49 “Enhanced MR Image Storage SOP Class” in 2002, which included the “MR Spectroscopy Information Object Definition” that is suitable for the storage and transfer of MRS data. This allows MRS data points, and associated localization volume



and acquisition information, to be archived to the picture archiving and communication system alongside the MRI, using a local network and the same protocols and infrastructure in place as in most radiology departments. Therefore, we recommend the use of the DICOM standard for storage and network transmission of the MRS data points and analysis results from the scanner, and strongly encourage MR and picture archiving and communication system vendors to implement the standard. For SVS, the storage of individual averages is recommended to aid retrospective correction of frequency and phase instabilities and the identification/removal of motion-corrupted averages. Standard DICOM tags should be used to store all important sequence and localization information, and the use of private tags for this information is strongly discouraged, as private tags cannot be guaranteed to be free from protected health information and are therefore automatically removed as part of the de-identification procedures required for clinical trials.

Although the DICOM-MRS format is essential for clinical purposes, we also recognize the importance of “raw” data formats. For instance, the data from each coil element need to be stored separately for researchers to develop and compare reconstruction methods, and the DICOM format may not be suitable for these purposes. For these, reconstruction research-orientated application formats, such as the ISMRM raw data format, are recommended for data export.<sup>126</sup>

### 3.6 | Reporting

The ideal for using MRS as a clinical biomarker would be the ability to report tissue metabolite levels fully, quantitatively, and independent of the scanner type or the pathology under investigation. In practice, limitations of SNR include the need for reasonable acquisition times, the need for voxels to contain mixed tissue types of variable relaxation times, and the effects of methodological variations due to differences in scanner software and hardware; these restrict convergence to the ideal. In addition, there may be reluctance to move too far away from a specific institutional MRS protocol and acquire new data that are no longer comparable to historical studies. Hence, pragmatically, our recommendations balance limited protocol variability with best practices of acquiring high-quality MRS data, avoiding a methodology that leads to extreme variation in MRS characteristics. Nevertheless, the appearance of the spectrum may still have characteristics that depend on the acquisition protocol, and the subsequent data processing may lead to further differences—all of which may affect visual or pattern recognition analyses. The most promising clinical applications for MRS have been described,<sup>1</sup> but further work is needed for the development of standardized MRS biomarkers that enable rigorous and robust multi-institutional use. Hence, it is essential that key details be provided

in MRS publications to enable appropriate comparisons among different studies and for meta-analyses, to better assess the efficacy of the proposed MRS biomarkers.

At the 2016 ISMRM workshop “MR Spectroscopy: From Current Best Practice to Latest Frontiers,” attendees were asked to comment on a set of minimum and recommended requirements for the reporting of MRS studies. Level 1 requirements were the parameters that are considered the minimum for proper and correct reporting of MRS studies by more than 80% of the attendees. Parameters that had between 40% and 80% support as relevant for inclusion in MRS reporting are ascribed as level 2. A detailed consensus on MRS reporting is currently being developed for an NMR in Biomedicine Special Issue (expected publication in late 2019); hence, only the outline of level 1 minimum requirements is included here (Supporting Information Section D) in relation to our consensus on <sup>1</sup>H MRS of the brain.

## 4 | SUMMARY AND CONCLUSIONS

Tables 1, 2, and 3 summarize SVS, 2D MRSI, and analysis/interpretation recommendations, respectively. To facilitate greater clinical utility of MRS, we encourage vendors to implement all recommendations as outlined here. We highlight the following 3 recommendations as being likely to have the greatest importance for improving routine clinical MRS and achieving reliable MRS results:

1. Implementation of a robust semi-LASER protocol to improve the localization of SVS and MRSI at 3 T;
2. Incorporation of simulated metabolite, lipid, and macromolecular basis sets in spectral analyses for more robust extraction of the maximum amount of metabolic information available; and
3. Use of optimized algorithms to perform time-efficient, robust, and high-quality automated shimming.<sup>123</sup>

These highlighted recommendations are all software-based and can therefore be implemented on almost all existing clinical scanners, significantly enhancing their MRS capabilities.

Although we have intentionally restricted the scope of our recommendations to the most common clinical field strengths of 1.5 T and 3 T, the same recommendations are also relevant to ultrahigh field (7 T and above), where reducing CSD and implementing robust shimming present significantly greater challenges.<sup>127</sup> Furthermore, a greater number of metabolites can be detected reliably at ultrahigh field, due to wider chemical shift dispersion, and the use of comprehensive simulated metabolite basis sets is required to capture the full metabolite profile.<sup>128</sup>

**TABLE 2** Two-dimensional MRSI acquisition and preprocessing consensus summary

Aspect	Consensus
Prelocalization method	CSD less than 2% per ppm. 3 T: Semi-LASER with OVS (preferred) or OVERPRESS with VSS. 1.5 T: Semi-LASER with OVS (preferred) or PRESS with VSS.
TE and TR	TE as short as possible (typically 30 ms). Longer TEs may be preferred for lactate detection (144 ns or 288 ms) and enhanced lipid suppression. TR = 1.5 seconds at 1.5 T, 2.0 seconds at 3 T.
Matrix dimensions, nominal voxel dimensions, and sampling parameters	16 × 16 matrix with 10-mm in-plane resolution and 15-mm slice thickness; 1 average per phase-encoding step. Spectral sampling of 1024 complex data points at 2000-Hz spectral width at 1.5 T or 3 T.
k-space sampling and preprocessing	2D phase-encoded Cartesian sampling over an elliptical or circular k-space mask. K-space zero-filling (interpolation) to twice the acquired number of points. Hamming filter. Reduction of subcutaneous lipid contamination (e.g., Papoulis-Gerchberg algorithm).
Water-reference acquisition	Should be acquired where possible. Collect with the same sequence parameters as the water-suppressed scan, but without water suppression. Typically, to reduce scan time, a lower resolution scan is acceptable and interpolated following acquisition to match the metabolite resolution.
B <sub>0</sub> shimming hardware	Second-order shim coils with adequately powered amplifiers are recommended at 1.5 T and 3 T.
B <sub>0</sub> shimming algorithm	Methods incorporating shim strength limits and instability countermeasures are preferred over unconstrained approaches.

**TABLE 3** Analysis and interpretation consensus summary

Aspect	Consensus
Spectral preprocessing	Time-domain apodization (line broadening) and zero-filling steps should not be applied before spectral fitting, although may aid visual interpretation. Water reference-based eddy-current correction <sup>42</sup> before fitting is recommended where possible.
Analysis methods	Methods should be fully automated, performing phasing, chemical shift calibration, and metabolite amplitude estimation without user intervention. The flexibility to be able to model typical baseline and linewidth variations is an essential requirement, which may be achieved using time or frequency-domain approaches.
Basis set	Methods that incorporate prior knowledge using a basis set are recommended over spectral integration or simple fitting of independent single peaks. Metabolite basis sets simulated from known <i>J</i> -coupling and chemical-shift values to match the acquisition protocol are recommended for analysis. Lipid basis signals should also be incorporated for tumor analysis and macromolecule signals for short-TE (< 80 ms) analyses.
Quality assessment	Single-peak metabolite and, where available, water linewidths should be measured at half height (FWHM) as part of an automated analysis pipeline. Metabolite or water linewidths less than 0.1 ppm are required for accurate analysis, and a metabolite SNR greater than 3 is the minimum criterion for determining the presence of a singlet. Visual assessment of spectral and fit quality is recommended, based on the combined display of the phased spectrum, fit, estimated baseline, and fit residual.

Consensus on appropriate experimental methodology is an evolving process, and we emphasize that this paper should not represent the final word on the topic. Our intention is to provide an assessment of the current state-of-the-art and

recommend improvements to MRS methodology and standardization, with a strong focus on clinical applications. However, variety is essential for fruitful developments of new and alternative methods, yielding the clinical workhorses of

the future. A current initiative will produce a special issue that will expand on this paper with a greater focus on ultra-high-field MRS and more novel methods.

In conclusion, a large body of research demonstrates that (1) robust, high-quality MRS data may be acquired with the hardware available on current clinical MR systems; and (2) many technical challenges of performing clinically useful SVS and MRSI at 1.5 T and 3 T can be overcome with software improvements applied to current scanner hardware. In this consensus paper, a series of methodological recommendations have been made to provide a degree of standardization and equivalency of methodology across all scanner platforms, and guidelines have been drawn up on the current best practices for clinical MRS.

## ACKNOWLEDGMENTS

The following authors drafted specific sections contained within this paper: Robert Bartha, In-Young Choi, Cristina Cudalbu, Anke Henning, Hoby P. Hetherington, Franklyn A. Howe, Kejal Kantarci, Dennis W. J. Klomp, Roland Kreis, Alexander P. Lin, Malgorzata Marjanska, Andrew A. Maudsley, Paul G. Mullins, Sarah J. Nelson, Gülin Öz, Julie W. Pan, Harish Poptani, Stefan Posse, Eva-Maria Ratai, and Martin Wilson. Figure 3 was provided by Yan Li (University of California, San Francisco). Martin Wilson, Franklyn A. Howe, and Gülin Öz played a primary role in editing the contributed text and drafting the final version of the manuscript.

## ORCID

Martin Wilson  <https://orcid.org/0000-0002-2089-3956>

Roland Kreis  <https://orcid.org/0000-0002-8618-6875>

Andrew A. Maudsley  <https://orcid.org/0000-0001-7653-3063>

Franklyn A. Howe  <https://orcid.org/0000-0002-7135-3351>

## REFERENCES

- Öz G, Alger JR, Barker PB, et al. Clinical proton MR spectroscopy in central nervous system disorders. *Radiology*. 2014;270:658–679.
- Di Costanzo A, Trojsi F, Tosetti M, et al. Proton MR spectroscopy of the brain at 3 T: an update. *Eur Radiol*. 2007;17:1651–1662.
- Frahm J, Merboldt KD, Hänicke W. Localized proton spectroscopy using stimulated echoes. *J Magn Reson*. 1987;72:502–508.
- Frahm J, Bruhn H, Gyngell ML, Merboldt KD, Hänicke W, Sauter R. Localized high-resolution proton NMR spectroscopy using stimulated echoes: initial applications to human brain in vivo. *Magn Reson Med*. 1989;9:79–93.
- Bottomley PA. Spatial localization in NMR spectroscopy in vivo. *Ann N Y Acad Sci*. 1987;508:333–348.
- Drost DJ, Riddle WR, Clarke GD. Proton magnetic resonance spectroscopy in the brain: report of AAPM MR Task Group #9. *Med Phys*. 2002;29:2177–2197.
- Ernst T, Chang L. Elimination of artifacts in short echo time 1H MR spectroscopy of the frontal lobe. *Magn Reson Med*. 1996;36:462–468.
- Moonen C, Sobering G, Van Zijl P, Gillen J, Von Kienlin M, Bizzi A. Proton spectroscopic imaging of human brain. *J Magn Reson*. 1992;98:556–575.
- Lange T, Dydak U, Roberts T, Rowley HA, Bjeljac M, Boesiger P. Pitfalls in lactate measurements at 3T. *Am J Neuroradiol*. 2006;27:895–901.
- Hyde JS, Jesmanowicz A, Froncisz W, Bruce Kneeland J, Grist TM, Campagna NF. Parallel image acquisition from noninteracting local coils. *J Magn Reson*. 1969;1986(70):512–517.
- Roemer PB, Edelstein WA, Hayes CE, Souza SP, Mueller OM. The NMR phased array. *Magn Reson Med*. 1990;16:192–225.
- Rodgers CT, Robson MD. Receive array magnetic resonance spectroscopy: whitened singular value decomposition (WSVD) gives optimal Bayesian solution. *Magn Reson Med*. 2010;63:881–891.
- Maril N, Lenkinski RE. An automated algorithm for combining multivoxel MRS data acquired with phased-array coils. *J Magn Reson Imaging*. 2005;21:317–322.
- Dong Z, Peterson B. The rapid and automatic combination of proton MRSI data using multi-channel coils without water suppression. *Magn Reson Imaging*. 2007;25:1148–1154.
- Vareth M, Lupo J, Larson P, Nelson S. A comparison of coil combination strategies in 3D multi-channel MRSI reconstruction for patients with brain tumors. *NMR Biomed*. 2018;31:e3929.
- Tkáč I, Öz G, Adriany G, Uğurbil K, Gruetter R. In vivo 1H NMR spectroscopy of the human brain at high magnetic fields: metabolite quantification at 4T vs. 7T. *Magn Reson Med*. 2009;62:868–879.
- Cudalbu C, Mlynárik V, Gruetter R. Handling macromolecule signals in the quantification of the neurochemical profile. *J Alzheimer's Dis*. 2012;31(Suppl 3):S101–S115.
- Gruetter R, Tkáč I. Field mapping without reference scan using asymmetric echo-planar techniques. *Magn Reson Med*. 2000;43:319–323.
- Shen J, Rothman DL, Hetherington HP, Pan JW. Linear projection method for automatic slice shimming. *Magn Reson Med*. 1999;42:1082–1088.
- Shen J, Rycyna RE, Rothman DL. Improvements on an in vivo automatic shimming method (FASTERMAP). *Magn Reson Med*. 1997;38:834–839.
- Gruetter R. Automatic, localized in vivo adjustment of all first- and second-order shim coils. *Magn Reson Med*. 1993;29:804–811.
- Gruetter R, Fast BC. Noniterative shimming of spatially localized signals. In vivo analysis of the magnetic field along axes. *J Magn Reson*. 1969;1992(96):323–334.
- Webb P, Macovski A. Rapid, fully automatic, arbitrary volume in vivo shimming. *Magn Reson Med*. 1991;20:113–122.
- Schneider E, Glover G. Rapid in vivo proton shimming. *Magn Reson Med*. 1991;18:335–347.
- Kanayama S, Kuhara S, Satoh K. In vivo rapid magnetic field measurement and shimming using single scan differential phase mapping. *Magn Reson Med*. 1996;36:637–642.
- Spielman DM, Adalsteinsson E, Lim KO. Quantitative assessment of improved homogeneity using higher-order shims

- for spectroscopic imaging of the brain. *Magn Reson Med.* 1998;40:376–382.
27. Haase A, Frahm J, Hänicke W, Matthaei D. 1H NMR chemical shift selective (CHESS) imaging. *Phys Med Biol.* 1985;30:341–344.
  28. Ogg RJ, Kingsley PB, Taylor JS. WET, a T1- and B1-insensitive water-suppression method for in vivo localized 1H NMR spectroscopy. *J Magn Reson B.* 1994;104:1–10.
  29. Tkáč I, Starcuk Z, Choi IY, Gruetter R. In vivo 1H NMR spectroscopy of rat brain at 1 ms echo time. *Magn Reson Med.* 1999;41:649–656.
  30. Howe FA, Barton SJ, Cudlip SA, et al. Metabolic profiles of human brain tumors using quantitative in vivo 1H magnetic resonance spectroscopy. *Magn Reson Med.* 2003;49:223–232.
  31. O'Connor JPB, Aboagye EO, Adams JE, et al. Imaging biomarker roadmap for cancer studies. *Nat Rev Clin Oncol.* 2017;14:169–186.
  32. Provencher SW. Estimation of metabolite concentrations from localized in vivo proton NMR spectra. *Magn Reson Med.* 1993;30:672–679.
  33. Young K, Soher BJ, Maudsley AA. Automated spectral analysis II: application of wavelet shrinkage for characterization of non-parameterized signals. *Magn Reson Med.* 1998;40:816–821.
  34. Ratiney H, Sdika M, Coenradie Y, Cavassila S, van Ormondt D, Graveron-Demilly D. Time-domain semi-parametric estimation based on a metabolite basis set. *NMR Biomed.* 2005;18:1–13.
  35. Wilson M, Reynolds G, Kauppinen RA, Arvanitis TN, Peet AC. A constrained least-squares approach to the automated quantitation of in vivo (1)H magnetic resonance spectroscopy data. *Magn Reson Med.* 2011;65:1–12.
  36. Govindaraju V, Young K, Maudsley AA. Proton NMR chemical shifts and coupling constants for brain metabolites. *NMR Biomed.* 2000;13:129–153.
  37. Govind V, Young K, Maudsley AA. Corrigendum: proton NMR chemical shifts and coupling constants for brain metabolites. Govindaraju V, Young K, Maudsley AA. *NMR Biomed.* 13: 129–153. *NMR Biomed.* 2000;2015(28):923–924.
  38. Young K, Govindaraju V, Soher BJ, Maudsley AA. Automated spectral analysis I: formation of a priori information by spectral simulation. *Magn Reson Med.* 1998;40:812–815.
  39. Wilson M, Davies NP, Sun Yu, et al. A comparison between simulated and experimental basis sets for assessing short-TE in vivo (1) H MRS data at 1.5 T. *NMR Biomed.* 2010;23:1117–1126.
  40. Kaiser LG, Young K, Matson GB. Numerical simulations of localized high field 1H MR spectroscopy. *J Magn Reson.* 2008;195:67–75.
  41. Seeger U, Klose U, Mader I, Grodd W, Nägele T. Parameterized evaluation of macromolecules and lipids in proton MR spectroscopy of brain diseases. *Magn Reson Med.* 2003;49:19–28.
  42. Klose U. In vivo proton spectroscopy in presence of eddy currents. *Magn Reson Med.* 1990;14:26–30.
  43. Kreis R. Issues of spectral quality in clinical 1H-magnetic resonance spectroscopy and a gallery of artifacts. *NMR Biomed.* 2004;17:361–381.
  44. Pedrosa de Barros N, Slotboom J. Quality management in in vivo proton MRS. *Anal Biochem.* 2017;529:98–116.
  45. Kyathanahally SP, Kreis R. Forecasting the quality of water-suppressed 1H MR spectra based on a single-shot water scan. *Magn Reson Med.* 2017;78:441–451.
  46. Kreis R. The trouble with quality filtering based on relative Cramér-Rao lower bounds. *Magn Reson Med.* 2016;75:15–18.
  47. Ernst T, Kreis R, Ross BD. Absolute quantitation of water and metabolites in the human brain. I: Compartments and water. *J Magn Reson Ser B.* 1993;102:1–8.
  48. Gasparovic C, Song T, Devier D, et al. Use of tissue water as a concentration reference for proton spectroscopic imaging. *Magn Reson Med.* 2006;55:1219–1226.
  49. Brown TR, Kincaid BM, Ugurbil K. NMR chemical shift imaging in three dimensions. *Proc Natl Acad Sci.* 1982;79:3523–3526.
  50. Maudsley AA, Hilal SK, Perman WH, Simon HE. Spatially resolved high resolution spectroscopy by “four-dimensional” NMR. *J Magn Reson.* 1983;51:147–152.
  51. Duijn JH, Matson GB, Maudsley AA, Weiner MW. 3D phase encoding 1H spectroscopic imaging of human brain. *Magn Reson Imaging.* 1992;10:315–319.
  52. Ebel A, Maudsley AA. Comparison of methods for reduction of lipid contamination for in vivo proton MR spectroscopic imaging of the brain. *Magn Reson Med.* 2001;46:706–712.
  53. Sabati M, Zhan J, Govind V, Arheart KL, Maudsley AA. Impact of reduced k-space acquisition on pathologic detectability for volumetric MR spectroscopic imaging. *J Magn Reson Imaging.* 2014;39:224–234.
  54. Pan JW, Lo K-M, Hetherington HP. Role of very high order and degree B0 shimming for spectroscopic imaging of the human brain at 7 tesla. *Magn Reson Med.* 2012;68:1007–1017.
  55. Dydak U, Weiger M, Pruessmann KP, Meier D, Boesiger P. Sensitivity-encoded spectroscopic imaging. *Magn Reson Med.* 2001;46:713–722.
  56. Ozturk-Isik E, Crane JC, Cha S, Chang SM, Berger MS, Nelson SJ. Unaliasing lipid contamination for MR spectroscopic imaging of gliomas at 3T using sensitivity encoding (SENSE). *Magn Reson Med.* 2006;55:1164–1169.
  57. Otazo R, Tsai S-YY, Lin F-HH, Posse S. Accelerated short-TE 3D proton echo-planar spectroscopic imaging using 2D-SENSE with a 32-channel array coil. *Magn Reson Med.* 2007;58:1107–1116.
  58. Tsai S-Y, Otazo R, Posse S, et al. Accelerated proton echo planar spectroscopic imaging (PEPSI) using GRAPPA with a 32-channel phased-array coil. *Magn Reson Med.* 2008;59:989–998.
  59. Ozturk-Isik E, Chen AP, Crane JC, et al. 3D sensitivity encoded ellipsoidal MR spectroscopic imaging of gliomas at 3T. *Magn Reson Imaging.* 2009;27:1249–1257.
  60. Bonekamp D, Smith MA, Zhu H, Barker PB. Quantitative SENSE-MRSI of the human brain. *Magn Reson Imaging.* 2010;28:305–313.
  61. Brown MA. Time-domain combination of MR spectroscopy data acquired using phased-array coils. *Magn Reson Med.* 2004;52:1207–1213.
  62. Birch R, Peet AC, Arvanitis TN, Wilson M. Sensitivity encoding for fast (1) H MR spectroscopic imaging water reference acquisition. *Magn Reson Med.* 2015;73:2081–2086.
  63. Skoch A, Jiru F, Bunke J. Spectroscopic imaging: basic principles. *Eur J Radiol.* 2008;67:230–239.
  64. Bonekamp D, Horska A, Jacobs MA, Arslanoglu A, Barker PB. Fast method for brain image segmentation: application to proton magnetic resonance spectroscopic imaging. *Magn Reson Med.* 2005;54:1268–1272.



65. Tal A, Kirov II, Grossman RI, Gonen O. The role of gray and white matter segmentation in quantitative proton MR spectroscopic imaging. *NMR Biomed.* 2012;25:1392–1400.
66. Du S, Mao X, Sajda P, Shungu DC. Automated tissue segmentation and blind recovery of (1)H MRS imaging spectral patterns of normal and diseased human brain. *NMR Biomed.* 2008;21:33–41.
67. Young K, Khetselius D, Soher BJ, Maudsley AA. Confidence images for MR spectroscopic imaging. *Magn Reson Med.* 2000;44:537–545.
68. Kalyanam R, Boutte D, Gasparovic C, Hutchison KE, Calhoun VD. Group independent component analysis of MR spectra. *Brain Behav.* 2013;3:229–242.
69. Menze BH, Kelm BM, Weber M-A, Bachert P, Hamprecht FA. Mimicking the human expert: pattern recognition for an automated assessment of data quality in MR spectroscopic images. *Magn Reson Med.* 2008;59:1457–1466.
70. Wright AJ, Arús C, Wijnen JP, et al. Automated quality control protocol for MR spectra of brain tumors. *Magn Reson Med.* 2008;59:1274–1281.
71. Maudsley AA, Darkazanli A, Alger JR, et al. Comprehensive processing, display and analysis for in vivo MR spectroscopic imaging. *NMR Biomed.* 2006;19:492–503.
72. Li Y, Osorio JA, Ozturk-Isik E, et al. Considerations in applying 3D PRESS H-1 brain MRSI with an eight-channel phased-array coil at 3 T. *Magn Reson Imaging.* 2006;24:1295–1302.
73. Tran T-K, Vigneron DB, Sailasuta N, et al. Very selective suppression pulses for clinical MRSI studies of brain and prostate cancer. *Magn Reson Med.* 2000;43:23–33.
74. Slotboom J, Mehlkopf AF, Bovée W. A single-shot localization pulse sequence suited for coils with inhomogeneous RF fields using adiabatic slice-selective RF pulses. *J Magn Reson.* 1969;1991(95):396–404.
75. Slotboom J, Bovée W. Adiabatic slice-selective rf pulses and a single-shot adiabatic localization pulse sequence. *Concepts Magn Reson.* 1995;7:193–217.
76. Garwood M, DelaBarre L. The return of the frequency sweep: designing adiabatic pulses for contemporary NMR. *J Magn Reson.* 2001;153:155–177.
77. Slotboom J, Mehlkopf AF, Bovee W. The effects of frequency-selective RF pulses on J-coupled spin-12 systems. *J Magn Reson Ser A.* 1994;108:38–50.
78. Scheenen T, Klomp D, Wijnen JP, Heerschap A. Short echo time 1H-MRSI of the human brain at 3T with minimal chemical shift displacement errors using adiabatic refocusing pulses. *Magn Reson Med.* 2008;59:1–6.
79. Öz G, Tkáč I. Short-echo, single-shot, full-intensity proton magnetic resonance spectroscopy for neurochemical profiling at 4 T: validation in the cerebellum and brainstem. *Magn Reson Med.* 2011;65:901–910.
80. Steinseifer IK, van Asten J, Weiland E, Scheenen T, Maas MC, Heerschap A. Improved volume selective (1) HMR spectroscopic imaging of the prostate with gradient offset independent adiabaticity pulses at 3 tesla. *Magn Reson Med.* 2015;74:915–924.
81. Andronesi OC, Gagoski BA, Sorensen AG. Neurologic 3D MR spectroscopic imaging with low-power adiabatic pulses and fast spiral acquisition. *Radiology.* 2012;262:647–661.
82. Deelchand DK, Joers JM, Snoussi K, et al. Across-vendor standardization of semi-LASER for single-voxel MRS at 3 Tesla. In: Proceedings of the ISMRM Workshop on MR Spectroscopy: From Current Best Practice to Latest Frontiers, Lake Constance, Germany; 2016.
83. Michaeli S, Garwood M, Zhu X-H, et al. Proton T2 relaxation study of water, N-acetylaspartate, and creatine in human brain using Hahn and Carr-Purcell spin echoes at 4T and 7T. *Magn Reson Med.* 2002;47:629–633.
84. Deelchand DK, Adanyeguh IM, Emir UE, et al. Two-site reproducibility of cerebellar and brainstem neurochemical profiles with short-echo, single-voxel MRS at 3T. *Magn Reson Med.* 2015;73:1718–1725.
85. Deelchand DK, Kantarci K, Öz G. Improved localization, spectral quality, and repeatability with advanced MRS methodology in the clinical setting. *Magn Reson Med.* 2018;79:1241–1250.
86. Terpstra M, Cheong I, Lyu T, et al. Test-retest reproducibility of neurochemical profiles with short-echo, single-voxel MR spectroscopy at 3T and 7T. *Magn Reson Med.* 2016;76:1083–1091.
87. Berrington A, Voets NL, Larkin SJ, et al. A comparison of 2-hydroxyglutarate detection at 3 and 7 T with long-TE semi-LASER. *NMR Biomed.* 2018;31.
88. Wijnen JP, van Asten J, Klomp D, et al. Short echo time 1H MRSI of the human brain at 3T with adiabatic slice-selective refocusing pulses; reproducibility and variance in a dual center setting. *J Magn Reson Imaging.* 2010;31:61–70.
89. Bednařík P, Moheet A, Deelchand DK, et al. Feasibility and reproducibility of neurochemical profile quantification in the human hippocampus at 3T. *NMR Biomed.* 2015;28:685–693.
90. Choi C, Ganji SK, DeBerardinis RJ, et al. 2-hydroxyglutarate detection by magnetic resonance spectroscopy in IDH-mutated patients with gliomas. *Nat Med.* 2012;18:624–629.
91. Li Y, Lafontaine M, Chang S, Nelson SJ. Comparison between short and long echo time magnetic resonance spectroscopic imaging at 3T and 7T for evaluating brain metabolites in patients with glioma. *ACS Chem Neurosci.* 2018;9:130–137.
92. Osorio JA, Xu D, Cunningham CH, et al. Design of cosine modulated very selective suppression pulses for MR spectroscopic imaging at 3T. *Magn Reson Med.* 2009;61:533–540.
93. Henning A, Schär M, Schulte RF, Wilm B, Pruessmann KP, Boesiger P. SELOVS: brain MRSI localization based on highly selective T1- and B1- insensitive outer-volume suppression at 3T. *Magn Reson Med.* 2008;59:40–51.
94. Stagg CJ, Knight S, Talbot K, Jenkinson M, Maudsley AA, Turner MR. Whole-brain magnetic resonance spectroscopic imaging measures are related to disability in ALS. *Neurology.* 2013;80:610–615.
95. Mansfield P. Spatial mapping of the chemical shift in NMR. *Magn Reson Med.* 1984;1:370–386.
96. Posse S, DeCarli C, Le Bihan D. Three-dimensional echo-planar MR spectroscopic imaging at short echo times in the human brain. *Radiology.* 1994;192:733–738.
97. Posse S, Tedeschi G, Risinger R, Ogg R, Le BD. High speed 1H spectroscopic imaging in human brain by echo planar spatial-spectral encoding. *Magn Reson Med.* 1995;33:34–40.
98. Posse S, Dager SR, Richards TL, et al. In vivo measurement of regional brain metabolic response to hyperventilation using magnetic resonance: proton echo planar spectroscopic imaging (PEPSI). *Magn Reson Med.* 1997;37:858–865.
99. Posse S, Otazo R, Caprihan A, et al. Proton echo-planar spectroscopic imaging of J-coupled resonances in human brain at 3 and 4 Tesla. *Magn Reson Med.* 2007;58:236–244.



100. Yung KT, Zheng W, Zhao C, Martínez-Ramón M, Van Der Kouwe A, Posse S. Atlas-based automated positioning of outer volume suppression slices in short-echo time 3D MR spectroscopic imaging of the human brain. *Magn Reson Med*. 2011;66:911–922.
101. Haupt CI, Schuff N, Weiner MW, Maudsley AA. Removal of lipid artifacts in 1H spectroscopic imaging by data extrapolation. *Magn Reson Med*. 1996;35:678–687.
102. Ebel A, Maudsley AA. Detection and correction of frequency instabilities for volumetric 1H echo-planar spectroscopic imaging. *Magn Reson Med*. 2005;53:465–469.
103. Sabati M, Sheriff S, Gu M, et al. Multivendor implementation and comparison of volumetric whole-brain echo-planar MR spectroscopic imaging. *Magn Reson Med*. 2015;74:1209–1220.
104. Maudsley AA, Domenig C, Sheriff S. Reproducibility of serial whole-brain MR spectroscopic imaging. *NMR Biomed*. 2010;23:251–256.
105. Donadieu M, Le Fur Y, Lecocq A, et al. Metabolic voxel-based analysis of the complete human brain using fast 3D-MRSI: proof of concept in multiple sclerosis. *J Magn Reson Imaging*. 2016;44:411–419.
106. Posse S, Otazo R, Dager SR, Alger J. MR spectroscopic imaging: principles and recent advances. *J Magn Reson Imaging*. 2013;37:1301–1325.
107. Ozhinsky E, Vigneron DB, Chang SM, Nelson SJ. Automated prescription of oblique brain 3D magnetic resonance spectroscopic imaging. *Magn Reson Med*. 2013;69:920–930.
108. Nelson SJ, Ozhinsky E, Li Y, Park I, Crane J. Strategies for rapid in vivo 1H and hyperpolarized 13C MR spectroscopic imaging. *J Magn Reson*. 2013;229:187–197.
109. Naressi A, Couturier C, Castang I, De Beer R, Graveron-Demilly D. Java-based graphical user interface for MRUI, a software package for quantitation of in vivo/medical magnetic resonance spectroscopy signals. *Comput Biol Med*. 2001;31:269–286.
110. Crane JC, Olson MP, Nelson SJ. SIVIC: open-source, standards-based software for DICOM MR spectroscopy workflows. *Int J Biomed Imaging*. 2013;2013:169526.
111. Starčuk Z, Starčukov J, Štrbák O, Graveron-Demilly D. Simulation of coupled-spin systems in the steady-state free-precession acquisition mode for fast magnetic resonance (MR) spectroscopic imaging. *Meas Sci Technol*. 2009;20:104033.
112. Smith SA, Levante TO, Meier BH, Ernst RR. Computer simulations in magnetic resonance. An object-oriented programming approach. *J Magn Reson Ser A*. 1994;106:75–105.
113. Simpson R, Devenyi GA, Jezzard P, Hennessy TJ, Near J. Advanced processing and simulation of MRS data using the FID appliance (FID-A)—an open source. *MATLAB-based toolkit. Magn Reson Med*. 2017;77:23–33.
114. Pedrosa de Barros N, McKinley R, Knecht U, Wiest R, Slotboom J. Automatic quality control in clinical 1H MRSI of brain cancer. *NMR Biomed*. 2016;29:563–575.
115. Near J, Edden R, Evans CJ, Paquin R, Harris A, Jezzard P. Frequency and phase drift correction of magnetic resonance spectroscopy data by spectral registration in the time domain. *Magn Reson Med*. 2015;73:44–50.
116. Öz G, Tkáč I, Charnas LR, et al. Assessment of adrenoleukodystrophy lesions by high field MRS in non-sedated pediatric patients. *Neurology*. 2005;64:434–441.
117. Wilson M. Robust retrospective frequency and phase correction for single-voxel MR spectroscopy. *Magn Reson Med*. 2019;81:2878–2886.
118. Hock A, MacMillan EL, Fuchs A, et al. Non-water-suppressed proton MR spectroscopy improves spectral quality in the human spinal cord. *Magn Reson Med*. 2013;69:1253–1260.
119. Zhang Y, Zhou J, Bottomley PA. Minimizing lipid signal bleed in brain (1) H chemical shift imaging by post-acquisition grid shifting. *Magn Reson Med*. 2015;74:320–329.
120. Bilgic B, Gagoski B, Kok T, Adalsteinsson E. Lipid suppression in CSI with spatial priors and highly undersampled peripheral k-space. *Magn Reson Med*. 2013;69:1501–1511.
121. Ma C, Lam F, Johnson CL, Liang Z-P. Removal of nuisance signals from limited and sparse 1H MRSI data using a union-of-subspaces model. *Magn Reson Med*. 2016;75:488–497.
122. Bilgic B, Chatnuntawech I, Fan AP, et al. Fast image reconstruction with L2-regularization. *J Magn Reson Imaging*. 2014;40:181–191.
123. Nassirpour S, Chang P, Fillmer A, Henning A. A comparison of optimization algorithms for localized in vivo B0 shimming. *Magn Reson Med*. 2018;79:1145–1156.
124. Juchem C, de Graaf RA. B0 magnetic field homogeneity and shimming for in vivo magnetic resonance spectroscopy. *Anal Biochem*. 2017;529:17–29.
125. Stockmann JP, Wald LL. In vivo B0 field shimming methods for MRI at 7 T. *Neuroimage*. 2018;168:71–87.
126. Inati SJ, Naegele JD, Zwart NR, et al. ISMRM Raw data format: a proposed standard for MRI raw datasets. *Magn Reson Med*. 2017;77:411–421.
127. Scheenen T, Heerschap A, Klomp D. Towards 1H-MRSI of the human brain at 7T with slice-selective adiabatic refocusing pulses. *MAGMA*. 2008;21:95–101.
128. van de Bank BL, Emir UE, Boer VO, et al. Multi-center reproducibility of neurochemical profiles in the human brain at 7T. *NMR Biomed*. 2015;28:306–316.
129. Kyathanahally SP, Döring A, Kreis R. Deep learning approaches for detection and removal of ghosting artifacts in MR spectroscopy. *Magn Reson Med*. 2018;80:851–863.
130. Ethofer T, Mader I, Seeger U, et al. Comparison of longitudinal metabolite relaxation times in different regions of the human brain at 1.5 and 3 Tesla. *Magn Reson Med*. 2003;50:1296–1301.
131. Landheer K, Sahgal A, Myrehaug S, Chen AP, Cunningham CH, Graham SJ. A rapid inversion technique for the measurement of longitudinal relaxation times of brain metabolites: application to lactate in high-grade gliomas at 3 T. *NMR Biomed*. 2016;29:1381–1390.
132. Wright PJ, Mougín OE, Totman JJ, et al. Water proton T1 measurements in brain tissue at 7, 3, and 1.5 T using IR-EPI, IR-TSE, and MPRAGE: results and optimization. *MAGMA*. 2008;21:121–130.

## SUPPORTING INFORMATION

Additional supporting information may be found online in the Supporting Information section at the end of the article.

**FIGURE S1** A selection of example spectra demonstrating the following features: good shimming (A), acceptable shimming (B), poor shimming and water suppression (C), out-of-volume lipid contamination (D), “ghost” artifact (E), and very poor shimming and water suppression (F). Further examples of poor spectra may be found in Refs 43 and 129

**FIGURE S2** Single-voxel spectroscopy planning with moderate CSD. Incorrect (A) and improved (C) voxel planning by reversal of the gradient polarity in the left–right direction; corresponding spectra are shown in (B) and (D). Lipid and metabolite excitation regions are shown in cream and orange, respectively

**FIGURE S3** The effect of TR on the SNR per unit time due to  $T_1$  saturation relative to that at TR = 6000 ms. On average, across the 4 metabolite curves shown, the maximum SNR per unit time is close to 1500 ms at 1.5 T and 2000 ms at 3 T. The metabolite  $T_1$  values used are the average values from different normal brain regions acquired with exactly the same acquisition and processing protocols at both 1.5 T and 3 T: tCho = 1103/1290 ms; tCr = 1232/1375 ms; and tNAA = 1303/1482 ms.<sup>130</sup> A lactate  $T_1$  of 2000 ms at 3 T for high-grade gliomas was used,<sup>131</sup> and this value scaled to 1754 ms for 1.5 T using a factor of 1.14, the average ratio of the normal-tissue metabolite  $T_1$  values at the 2 field strengths

**FIGURE S4** Effect of  $T_1$  saturation on tissue water signals and main metabolite signals and clinically relevant metabolite ratios. A TR of 6000 ms is required to maintain the signals shown within 95% of their unsaturated values. At 1.5 T, the  $T_1$  values of 3 key metabolites and gray matter are similar, and although they are more dispersed at 3 T, they have less variability than that for tissue-water  $T_1$ . Apart from lactate, the saturation curves for signal from pathological tissues are not shown, but pathological tissue with increased water content could have a water-saturation curve that is similar to that of lactate (see text for discussion on metabolite  $T_1$  values in pathological tissue). Tissue-water  $T_1$  relaxation times used for 1.5 T/3 T calculations were white matter = 650/840 ms; gray matter = 1200/1600 ms.<sup>132</sup> Metabolite  $T_1$  values were those used in Supporting Information Figure S3

**How to cite this article:** Wilson M, Andronesi O, Barker PB, et al. Methodological consensus on clinical proton MRS of the brain: Review and recommendations. *Magn Reson Med*. 2019;00:1–24. <https://doi.org/10.1002/mrm.27742>